AD-A128 902 ON THE PREDICTION OF THE LATERAL/DIRECTIONAL CHARACTERISTICS OF DISTRIBUT. (U) KUHN (RICHARD E) NEWPORT NEWS VA R E KUHN DEC 82 NADC-81275-60 1/1

UNCLASSIFIED N62269-82-C-0220 F/G 1/1 NL

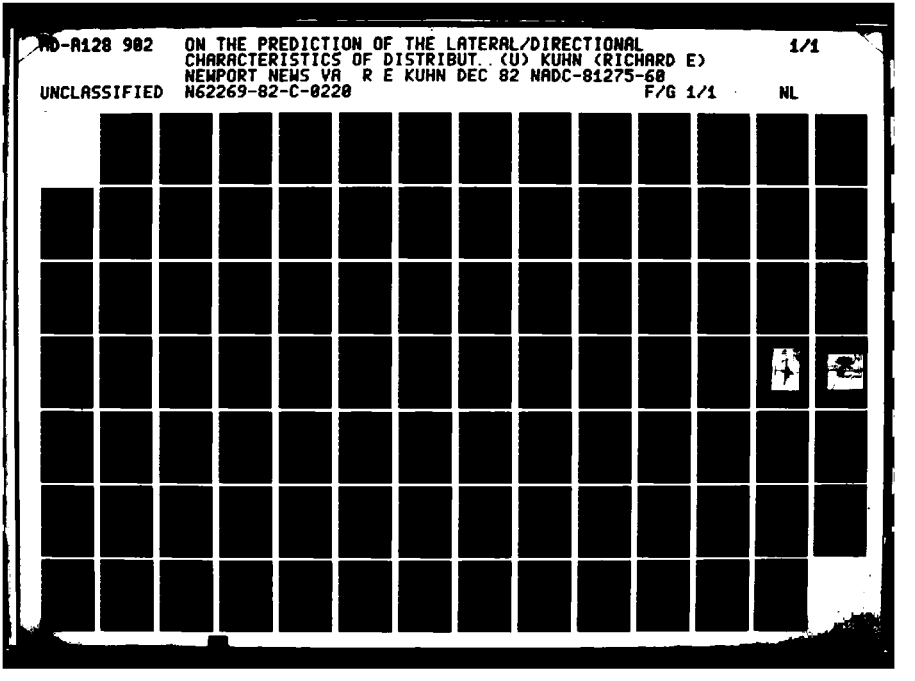

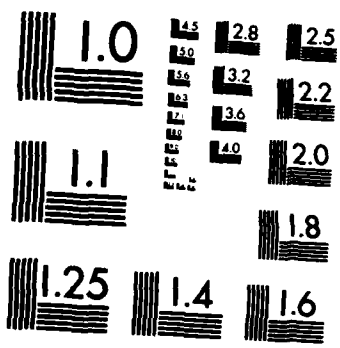

REPORT NO. NADC-81275-60

ON THE PREDICTION OF THE LATERAL/DIRECTIONAL CHARACTERISTICS OF DISTRIBUTED JET STOL CONFIGURATIONS

Richard E. Kuhn
V/STOL CONSULTANT
111 Mistletoe Drive
Newport News, VA 23606

DECEMBER 1982

FINAL REPORT
AIRTASK NO. A03V-320D/001B/7F41-400-000
Contract No. N62269-82-C-0220

APPROVED FOR PUBLIC RELEASE; DISTRIBUTION UNLIMITED

Prepared for
Aircraft and Crew Systems Technology Directorate (Code 6053)
NAVAL AIR DEVELOPMENT CENTER
Warminster, PA 18974

N O T I C E S

REPORT NUMBERING SYSTEM - The numbering of technical project reports issued by the Naval Air Development Center is arranged for specific identification purposes. Each number consists of the Center acronym, the calendar year in which the number was assigned, the sequence number of the report within the specific calendar year, and the official 2-digit correspondence code of the Command Office or the Functional Directorate responsible for the report. For example: Report No. NADC-78015-20 indicates the fifteenth Center report for the year 1978, and prepared by the Systems Directorate. The numerical codes are as follows:

CODE	OFFICE OR DIRECTORATE
00	Commander, Naval Air Development Center
01	Technical Director, Naval Air Development Center
02	Comptroller
10	Directorate Command Projects
20	Systems Directorate
30	Sensors & Avionics Technology Directorate
40	Communication & Navigation Technology Directorate
50	Software Computer Directorate
60	Aircraft & Crew Systems Technology Directorate
70	Planning Assessment Resources
80	Engineering Support Group

PRODUCT ENDORSEMENT - The discussion or instructions concerning commercial products herein do not constitute an endorsement by the Government nor do they convey or imply the license or right to use such products.

APPROVED BY: _____ DATE: 19 April 1983

T. J. GALLAGHER
CAPT, MSC, USN

SECURITY CLASSIFICATION OF THIS PAGE (When Data Entered)

REPORT DOCUMENTATION PAGE	READ INSTRUCTIONS BEFORE COMPLETING FORM
1. REPORT NUMBER: NADC-81275-60	2. GOVT ACCESSION NO. / 3. RECIPIENT'S CATALOG NUMBER
4. TITLE (and Subtitle): ON THE PREDICTION OF THE LATERAL DIRECTIONAL CHARACTERISTICS OF DISTRIBUTED JET STOL CONFIGURATIONS	5. TYPE OF REPORT & PERIOD COVERED: Final technical report 6. PERFORMING ORG. REPORT NUMBER
7. AUTHOR(s): Richard E. Kuhn	8. CONTRACT OR GRANT NUMBER(s): N62269-82-C-0220
9. PERFORMING ORGANIZATION NAME AND ADDRESS: Richard E. Kuhn, Inc. V/STOL Consultant 111 Mistletoe Drive Newport News, Va. 23606	10. PROGRAM ELEMENT, PROJECT, TASK AREA & WORK UNIT NUMBERS: AIRTASK NO. A03V-320D/001B/ 7F41-400-000
11. CONTROLLING OFFICE NAME AND ADDRESS: Naval Air Development Center Warminister, Pennsylvanis 18974	12. REPORT DATE: December 1982 13. NUMBER OF PAGES: 84
14. MONITORING AGENCY NAME & ADDRESS(if different from Controlling Office)	15. SECURITY CLASS. (of this report): Unclassified 15a. DECLASSIFICATION/DOWNGRADING SCHEDULE

16. DISTRIBUTION STATEMENT (of this Report)

17. DISTRIBUTION STATEMENT (of the abstract entered in Block 20, if different from Report)

Approved for Public Release: Distribution Unlimited

18. SUPPLEMENTARY NOTES

19. KEY WORDS (Continue on reverse side if necessary and identify by block number)

STOL	EBF
Jet flap	USB
Lateral/Directional Characteristics	IBF
Directional Stability	CCW
Dihedral Effect	

20. ABSTRACT (Continue on reverse side if necessary and identify by block number)

A method for estimating the lateral/directional stability characteristics of jet flap STOL transport configurations at high power-on lift coefficients is presented. In addition to inducing a large stabilizing sidewash at the vertical tail powered lift reduces the directional instability contribution of the wing/body, increases the wing body side force and tends to reduce (depending on the amount of geometric dihedral incorporated) the high level of effective dihedral normally associated with swept wings at high lift coefficients.

DD FORM 1 JAN 73 1473 EDITION OF 1 NOV 65 IS OBSOLETE
S/N 0102-LF-014-6601

SECURITY CLASSIFICATION OF THIS PAGE (When Data Entered)

TABLE OF CONTENTS

LIST OF FIGURES

LIST OF FIGURES

LIST OF FIGURES

NOTATION

The data in this paper are referred to the stability axis system.

A	aspect ratio
A_e	jet exit area, m
b	wing span, m
b_f	flap span, m
b_j	effective span of jet flap system, m; see fig. 17
C_L	lift coefficient, lift/qS
C_{L_o}	power lift coefficient, $C_{L_o} = \Delta(C_L)_\alpha + \Delta(C_L)_f$
$\Delta(C_L)_\alpha$	increment of lift coefficient due to angle of attack
ΔC_{L_f}	increment of lift coefficient due to flap deflection
ΔC_{L_μ}	increment of lift coefficient due to blowing, $\Delta C_{L_\mu} = C_L - C_{L_o}$
C_ℓ	rolling moment of coefficient, rolling moment/qSb
C_{ℓ_β}	effective dihedral parameter, $\partial C_\ell / \partial \beta$
$(C_{\ell_{\beta_o}})_D$	DATCOM estimate of effective dihedral parameter at zero lift; tail off
$(C_{\ell_\beta}/C_L)_D$	DATCOM estimate of variation of effective dihedral parameter with lift coefficient; tail off
$\Delta C_{\ell_{\beta_f}}$	increment of effective dihedral parameter due to flap deflection
$\Delta C_{\ell_{\beta_i}}$	increment of effective dihedral parameter due to inlet flow
$\Delta C_{\ell_{\beta_\mu}}$	increment of effective dihedral parameter due to blowing

NOTATION (Continued)

C_n	yawing moment coefficient, yawing moment/qSb
C_{n_β}	directional stability parameter, $\partial C_n/\partial\beta$
$C_{n_{\beta_D}}$	DATCOM estimate of directional stability parameter; tail off
$\Delta C_{n_{\beta_o}}$	increment of directional stability parameter due to lift coefficient; power off
$\Delta C_{n_{\beta_i}}$	increment of directional stability parameter due to inlet flow
$\Delta C_{n_{\beta_\mu}}$	increment of directional stability parameter due to blowing
$\Delta C_{n_{\beta_t}}$	increment of directional stability due to the tail
C_Y	side force coefficient, side force/qS
C_{Y_β}	side force parameter, $\partial C_Y/\partial\beta$
$C_{Y_{\beta_D}}$	DATCOM estimate of side force parameter; tail off
$\Delta C_{Y_{\beta_o}}$	increment of side force parameter due to lift coefficient; power off
$\Delta C_{Y_{\beta_i}}$	increment of side force parameter due to inlet flow
$\Delta C_{Y_{\beta_\mu}}$	increment of side force parameter due to blowing
C_μ	jet flap momentum coefficient, $\dot{m}V_e/qS$

NOTATION (Continued)

K_{ℓ_Λ}	constant used in calculating effect of sweep on $\Delta C_{\ell_{\beta_\mu}}$; see fig. 15
K_{ℓ_θ} and K_θ	constants used in calculating effect of jet sheet deflection on $\Delta C_{\ell_{\beta_\mu}}$; see fig. 14
K_{ℓ_A}	constant used in calculating effect of aspect ratio on $\Delta C_{\ell_{\beta_\mu}}$; see fig. 13
K_{ℓ_Γ}	constant used in calculating effect of dihedral on $\Delta C_{\ell_{\beta_\mu}}$; see fig. 13
K_σ	constant used in calculating sidewash at tail; see fig. 20
$\dot{m}_i$	inlet mass flow
$\dot{m}_i/\dot{m}_e$	ratio of inlet to exit mass flow
q	freestream dynamic pressure, N/m^2
S	wing area, m^2
V	freestream velocity, m/s
V_e	jet exit velocity, m/s
x_i	longitudinal distance from moment reference point to inlet face; positive forward, m
x_t	longitudinal distance from moment reference point to aerodynamic center of vertical tail; positive rearward, m
x_j	longitudinal distance from trailing edge of jet flap to aerodynamic center of vertical tail; positive rearward, m
z_i	vertical distance from moment reference point to center of inlet face; positive upward, m
z_t	vertical distance from moment reference point to aerodynamic center of vertical tail; positive upward, m

NOTATION (Continued)

α	angle of attack, deg.
β	angle of sideslip, deg.
$\Lambda_{c/4}$	sweepback angle of wing quarter chord line, deg.
$\Lambda_{c/2}$	sweepback angle of wing mid chord line, deg.
Γ	dihedral, deg.
δ_f	flap deflection, deg.
ρ_e/ρ_o	ratio of exit flow density to freestream density
θ	jet sheet deflection angle, deg.

SUMMARY

This study has examined the possibility of developing a method for estimating the lateral/directional stability characteristics of distributed jet (jet flap) STOL configurations and developed a method that is believed to account for the major effects of operating at high power-on lift coefficients. In addition to inducing a large stabilizing side wash at the vertical tail, powered lift reduces the directional instability contribution of the wing/body, increases the side force due to sideslip and tends to reduce (depending on the amount of geometric dihedral incorporated) the high level of effective dihedral normally associated with swept wings at high lift coefficients.

The method is intended for use only in preliminary design and not as a substitute for a carefully conducted wind tunnel program which will still be required in the development of any powered lift aircraft. The data base on which the method is based is primarily from model tests of high wing transport configurations. The effects of moving the wing to a low position are unknown and application of the method to configurations with wings having aspect ratios less than about 7 and sweep angles above about 30 degrees should be made with caution.

INTRODUCTION

A number of concepts have been developed that use power to augment wing lift to achieve STOL performance. They use various approaches to distribute the exhaust flow from the engine, or high pressure air taken from the engine, over a significant part of the wing span. These distributed jet STOL concepts include: the Internally Blown Flap (IBF) in which high pressure air from the engines is ducted to a spanwise nozzle at the flap knee, the Externally Blown Flap (EBF) in which the engines are mounted under the wing and the engine exhaust is blown at and through the slotted flaps, the Upper Surface Blowing (USB) concept in which the engines are mounted on the top of the wing and the exhaust is directed and spread over the top of the wing and flap system, and the Circulation Control Wing (CCW) concept in which high pressure air from the engines is ducted to the wing trailing edge and exhausted over a small radius cylinder that forms the wing trailing edge. All of these concepts control flow separation of the flaps as well as produce a deflected jet sheet that generate lift significantly greater than can be obtained with mechanical flaps.

The aerodynamic effects that act to produce the augmented lift also affect the lateral/directional characteristics of these configurations. A number of investigations have shown large effects of power-on directional stability and dihedral effect. The present study was undertaken to attempt to develop a method for estimating the static lateral/directional characteristics of these various STOL concepts. The method is based on an empirical correlation of the available data.

The present method is intended for use only in preliminary design work and to give a general indication of the effects of the primary configuration variables. The aerodynamic characteristics of STOL configurations are a complex function of many configuration variables and the development of any distributed jet STOL aircraft will require careful experimental investigations to accurately determine the lateral/directional forces and moments.

ACKNOWLEDGEMENTS

This work was supported by the Naval Air Development Center (NADC) in connection with the development of their V/STOL Aerodynamics and Stability and Control Manual (ref. 1). Appreciation is expressed to Mr. Campbell Henderson of NADC under who's technical direction the manual is being developed for his advice, suggestions, and encouragement.

Special appreciation is expressed to the Boeing Military Airplane Company, the Douglas Aircraft Company, the Convair Div. of General Dynamics, and the David Taylor Naval Ship R&D Center who supplied unpublished data from wind tunnel tests of models of the YC-14, YC-15, QSAR, and the A-6 CCW demonstrator airplane and related research models.

AVAILABLE METHODS

The V/STOL Aerodynamics and Stability and Control Manual (ref. 1) being developed by the Naval Air Development Center is intended to provide simple methods for estimating the aerodynamic characteristics of V/STOL and STOL aircraft. The concept of the manual is to develop and present methods of the type presented in the USAF DATCOM (ref. 2) (i.e., methods that can be easily handled with hand calculators) that extend the methodology into the hover and low speed modes of flight. The present study was undertaken to extend the DATCOM methods for estimating the sideslip derivatives C_{Y_β}, C_{n_β}, and C_{ℓ_β} to cover jet flap STOL configurations operating at high lift coefficients.

The present DATCOM method (ref. 2) is applicable only to the cruise configuration. Methods for estimating the effects of flap deflection and power are not included.

In the early 1970's Convair and Rockwell, under USAF sponsorship, conducted extensive programs to study and develop methods for estimating the aerodynamic characteristics of STOL aircraft. Internally Blown Flap (IFB), Externally Blown Flap (EBF), and vectored thrust concepts were covered but most emphasis was placed on the EBF concept and on the longitudinal characteristics.

The methods developed by Convair (ref. 3) and Rockwell (ref. 4) for estimating the lateral/directional characteristics produce significantly different results. For example, the Rockwell method (ref. 4) estimates the rolling moment due to sideslip C_{ℓ_β} simply by extending the DATCOM estimate

of the rolling moment per unit lift coefficient (C_{ℓ_β}/C_L) to the flaps deflected power on lift coefficient. Thus, the Rockwell method predicts very large negative values of C_{ℓ_β}. The Convair method (ref. 3) on the other hand provides for separate estimates for the effects of flap deflection and power, both of which yield positive increments of C_{ℓ_β} and, therefore, predicts much less dihedral effect than the Rockwell method. As will be shown later, the difference between the methods is largely due to the geometric dihedral of the models that provided the data bases for the two methods. The Rockwell data base was obtained on models with zero dihedral while the Convair data base was obtained on models with negative geometric dihedral.

METHOD DEVELOPMENT

The data base examined in the present study is presented in references 3 to 31 and contains data not available at the time of the Rockwell and Convair studies (refs. 3 and 4). Unfortunately, not all of these data were useful in developing the estimating method. Many studies did not include tail off data so that the wing-body and tail contributions could be examined separately and some did not even include power off cruise configuration (flaps retracted) data so that the applicability of the present DATCOM method to that configuration could be checked. Nevertheless, most provide some insight and were useful in checking the method developed in this study.

Wing-Body Contribution

The process used in this study was to examine the wing-body (tail off) data and the tail contributions separately. The wing-body data will be discussed first.

Typical Wing-body data for two configurations (and sketches of those configurations) are presented in figures 1 to 4 along with estimates from DATCOM and from the method developed in the present study. In general, flap deflection and power both produce an increase in side force (more negative values of C_{Y_β}) and a stabilizing contribution to directional stability (positive increment in C_{n_β}). For these two configurations which had essentially the same wing planforms the effect of flap deflection on dihedral effect depend on the wing geometric dihedral. With negative dihedral (fig. 2) flap deflection produces a positive increment in C_{ℓ_β}.

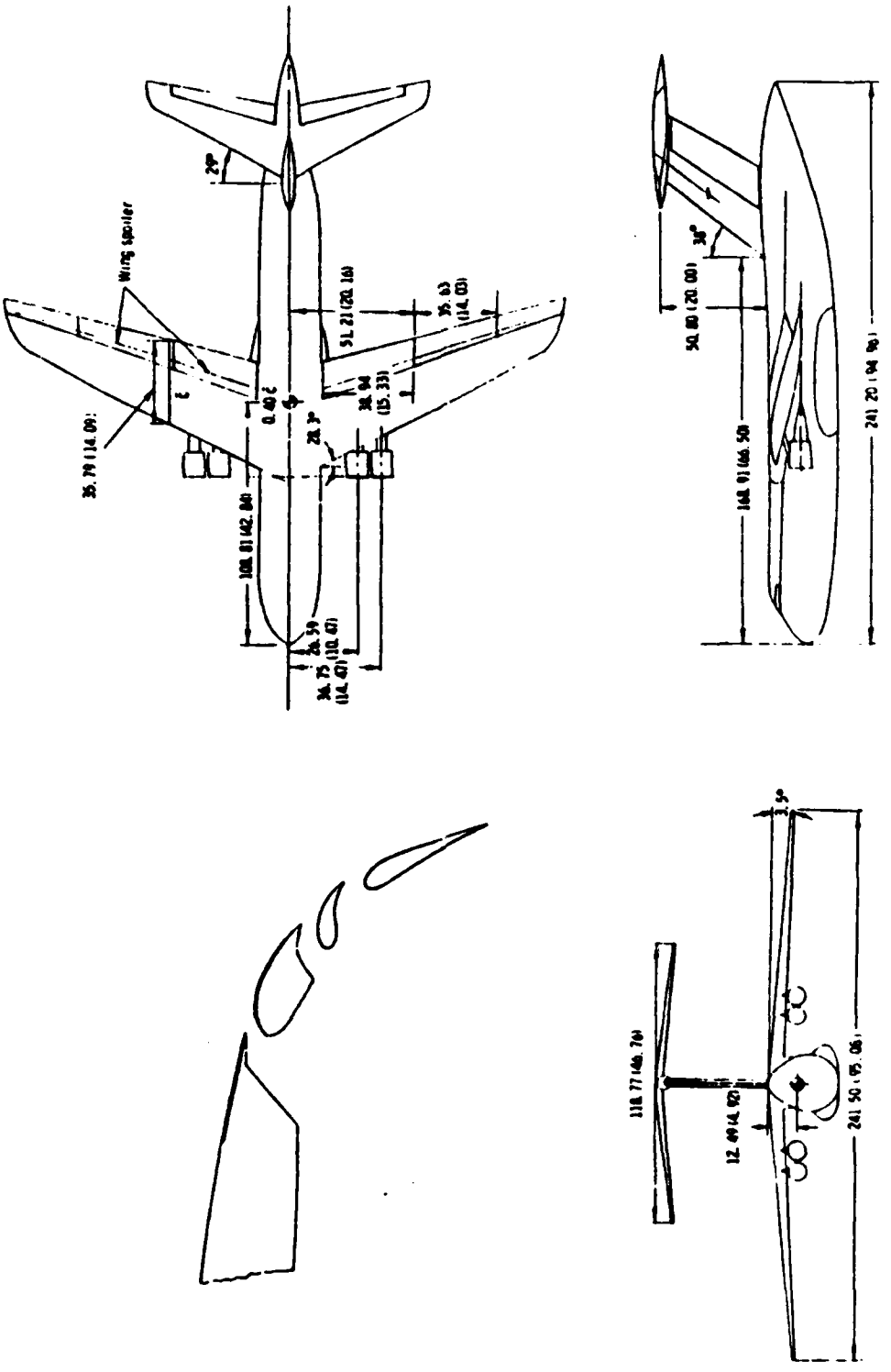

Figure 1 EFB Configuration of Ref. 10 and 11.
$A = 7.23$ $\Lambda_{c/2} = 22$ $\Gamma = -3.5$

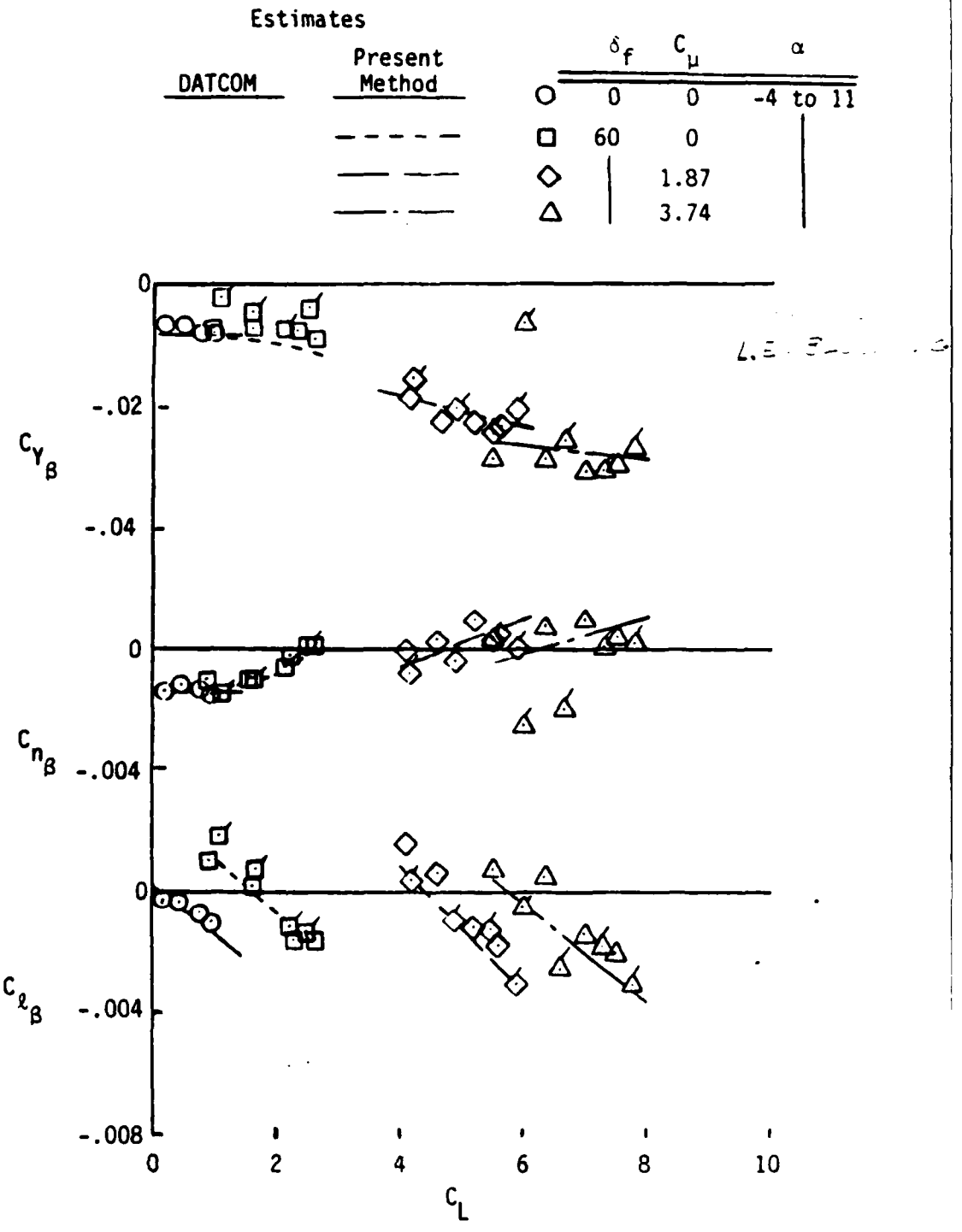

Figure 2 Wing-Body Data for the Configuration of Ref. 10 and Comparison with Estimates.

$A = 7.23 \quad \Lambda_{c/2} = 22 \quad \Gamma = -3.5$

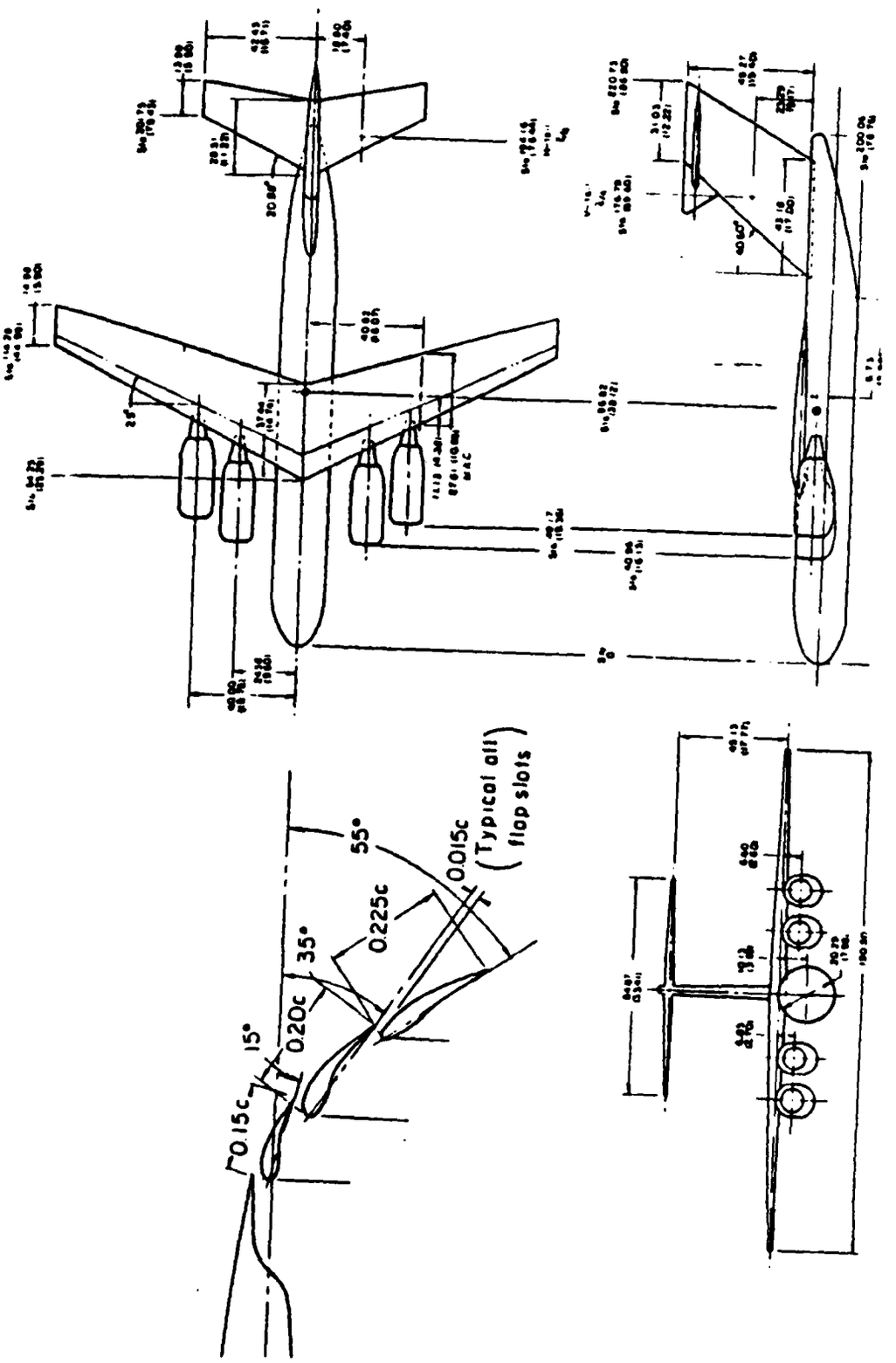

Figure 3 Configuration of EBF Models of Ref. 17 and 18.
$A = 7.0$ $\Lambda_{c/2} = 22$ $\Gamma = 0$

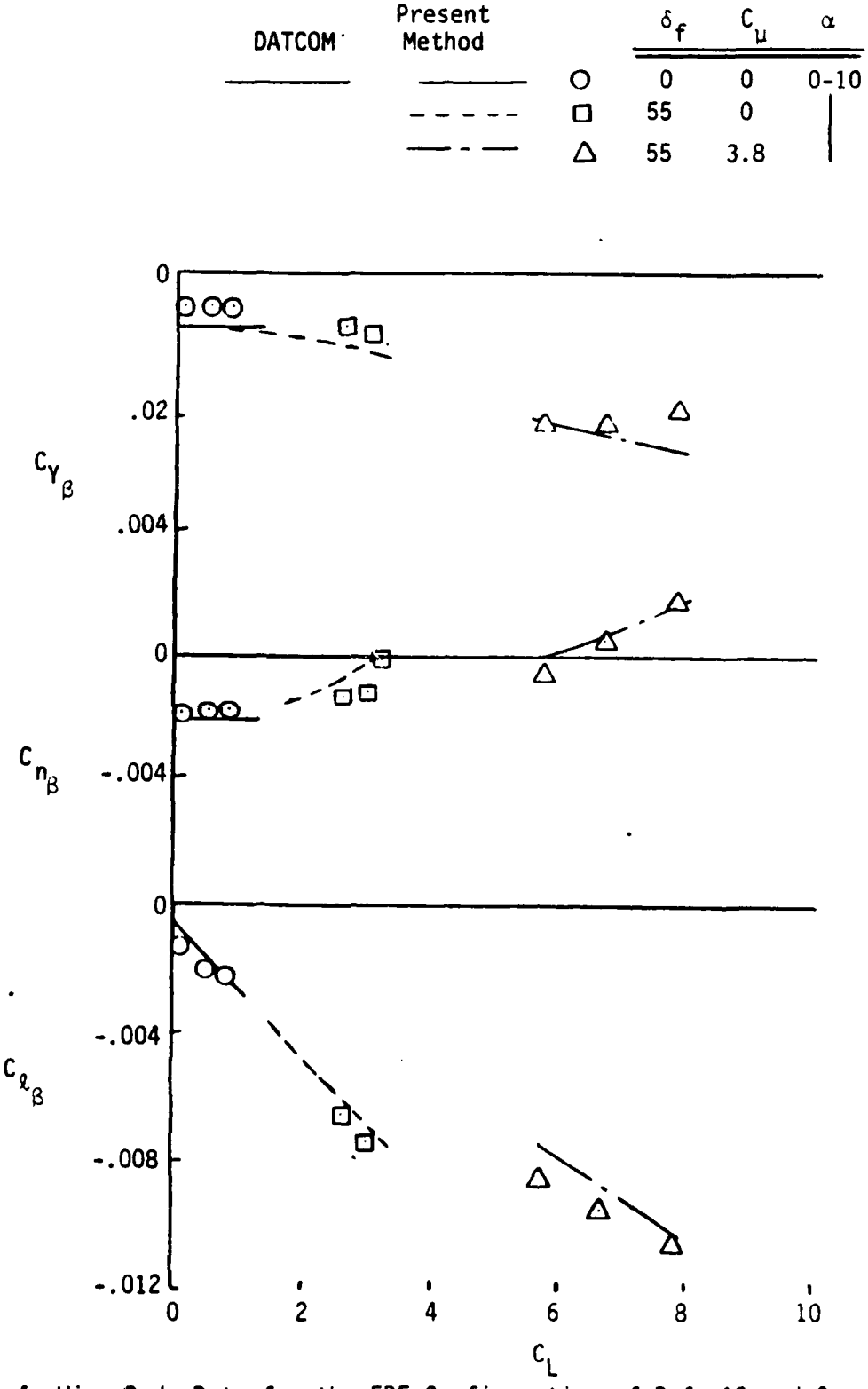

Figure 4 Wing-Body Data for the EBF Configuration of Ref. 18 and Comparison With Estimates.

$A = 7.0 \quad \Lambda_{c/2} = 22 \quad \Gamma = 0$

However, with zero dihedral (fig. 4) C_{ℓ_β} continues to increase negatively as lift coefficient is increased by flap deflection. The data obtained are essentially an extension of the DATCOM estimate to the higher lift coefficients. For both configurations, power produced positive increments of C_{ℓ_β} relative to those that would be obtained by extending the DATCOM estimate.

Comparison of the estimates made using the method developed in this study with the data in figures 2 and 4 give an idea of the accuracy of the method. More extensive comparisons will be given in a later section.

The available data usually contained a significant amount of scatter as shown in figure 2. In this case, the model was fitted with both a leading edge slat and blowing on the wing leading edge in an attempt to increase the lift generated. The data points shown by the flagged symbols were taken with both the slat and blowing and show slightly higher lifts than the plain symbols which were obtained with slat alone. Other than the small effect on lift, the small amount of blowing used would not be expected to affect the lateral/directional data and the differences shown are attributed to data scatter. For most of the other configurations, much more limited lateral/directional data were available and care had to be taken not to confuse data scatter with legitimate effects of geometric variables or operating conditions.

In general, the usual geometric parameters: aspect ratio, sweep, dihedral, and flap span were found to be significant to the lateral directional characteristics. Both the blowing momentum coefficient and the lift coefficient and various breakdowns of the lift coefficient were examined to determine appropriate correlating factors. It was found that the lateral/

directional characteristics could be correlated adequately with the power off lift (C_{L_o}), the lift increment due to flap deflection (ΔC_{L_f}) (needed only in estimating $\Delta C_{\ell_{\beta_f}}$) and the lift increment due to power (ΔC_{L_μ}) and that the momentum coefficient did not enter directly. Initially, the lift due to power (ΔC_{L_μ}) was broken down into the direct thrust component and the induced lift component. However, this added some complexity to the method and did not produce as good a correlation as that obtained using the lumped lift coefficient increment (ΔC_{L_μ}) which contains both the direct thrust component and the induced lift. The problem was probably due to inaccuracies in estimating the thrust deflection (to calculate the direct thrust component) for many of the sets of data which did not present the static thrust deflection data for their configuration.

Side Force

It was found that the side force parameter C_Y can be estimated by the expression

$$C_{Y_\beta} = C_{Y_{\beta_D}} + \Delta C_{Y_{\beta_o}} + \Delta C_{Y_{\beta_i}} + \Delta C_{Y_{\beta_\mu}}$$

where

$C_{Y_{\beta_D}}$ is the DATCOM estimate from section 5.2.1.1 (including nacelles)

$\Delta C_{Y_{\beta_o}}$ is the increment due to lift, power off

$\Delta C_{Y_{\beta_i}}$ is the increment due to inlet flow

and $\Delta C_{Y_{\beta_\mu}}$ is the increment due to blowing.

The DATCOM method for estimating C_{Y_β} is based on the fuselage side force adjusting for wing height and is appropriate at zero angle of attack. The side force contribution of the nacelles should also be included in this estimate, particularly for the EBF and USB configurations where the nacelles are large, and can contribute up to 40 percent of the zero lift side force. Their contribution should be estimated by treating them as small fuselages using the DATCOM method and their contribution added to the fuselage contribution to make up the estimate of $C_{Y_{\beta_D}}$.

Effect of Lift

Toll and Queijo in reference 5, using a simple strip theory, developed expressions for the side force contribution of swept wings at an angle of attack. This side force is due to the lateral cant of the resultant force vectors on the panels of a swept wing at combined angles of attack and sideslip. The resulting expressions are included in the DATCOM in section 5.1.1.1 but are seldom applied because this contribution is a function of C_L^2 and at lift coefficients appropriate to cruise configurations the contribution is negligible. With the flaps deflected, however, power off lift coefficients over 3 can be reached and this term should be significant.

Figure 5 presents the increments of side force parameter $C_{Y_{\beta_O}}$ as a function of lift coefficient squared for a variety of configurations. This increment was obtained by subtracting the value of C_{Y_β} at zero lift (using faired data) from the power off data at lift. Figure 5 shows a good correlation but all the values are negative rather than positive as predicted by reference 5. Also $C_{Y_{\beta_O}}$ appears to be independent of wing

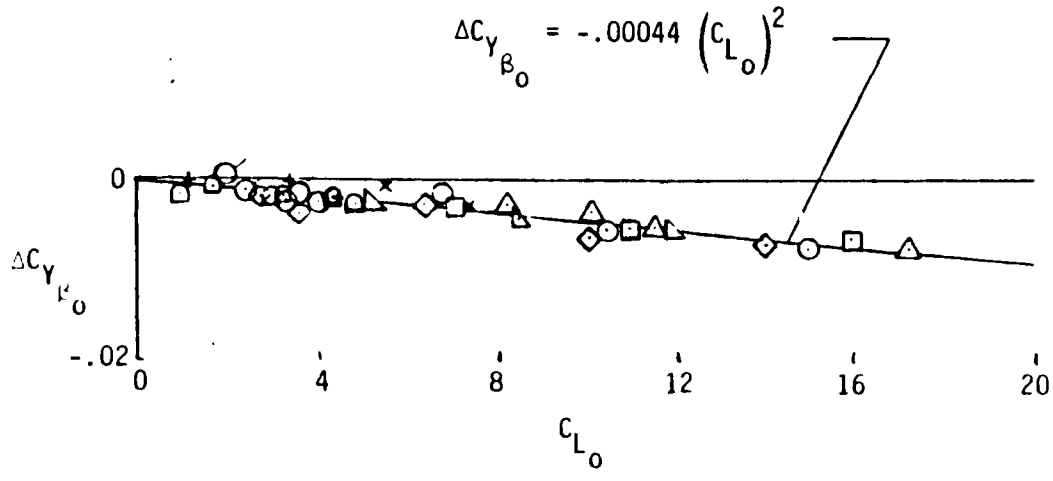

	Λ	A	Γ	Ref.	Flaps
○	22	8	-3.5		Slotted
□		9.52			
◇		7.14			
△	9.5	8		16	
△	32	8			
⌂	21.7	7.23		10	
×	3	7	2.8	13	
+	1.5	7	0	19	
◇	24.3	7	0	23	
○	22	8	-3.5	16	Plain

NADC 81275-60

Figure 5 Effect of Flaps on C_{Y_β}; Power Off

configuration rather than a function of sweep and aspect ratio as predicted by reference 5, thus suggesting that this increment of the side force parameter may be a lift induced side load on the fuselage and that the effects predicted by reference 5 may be submerged in these data. Also, it should be noted that all the data used in the present study were for high wing configurations (the analysis of ref. 5 is for wing alone) and the effects of mid or low wing placement are unknown.

For the present method, the increment of the side force parameter due to lift is given by:

$$\Delta C_{Y_{\beta_o}} = -0.00044(C_{L_o})^2$$

Effect of Inlet Flow

The effects of power on the side force parameter arise from two sources: the effects of inlet flow and the effects of blowing or jet flap action.

The inlet contribution to the side force parameter results from turning the flow into the inlets when the configuration is at a sideslip angle. The side force is simply the inlet momentum drag multiplied by the sin of the sideslip angle. In terms of the side force parameter, the increment due to inlet flow is given by:

$$\Delta C_{Y_{\beta_i}} = -\frac{\dot{m}V}{qs} \quad \frac{1}{57.3}$$

Unfortunately, the inlet mass flow associated with the lateral/directional data is not presented in most of the references available.

However, most of the engine simulators used in testing of small scale models were either ejectors or fans operating at relatively low pressure ratios. The approximate ratio of inlet to exit mass flow ratios for these engine simulators are known and the inlet contribution can be approximated by:

$$\Delta C_{Y_{\beta_i}} = \frac{\sqrt{C_\mu}}{qs} \frac{\dot{m}_i}{\dot{m}_e} \sqrt{\frac{2A_e}{S} \frac{\rho_e}{\rho_o}}$$

Fortunately, the inlet contribution to the side force parameter is small and any errors introduced by approximations of the mass flow ratio are believed to be small.

Effect of Blowing

The increments due to jet flap action are presented in figure 6 and were obtained by subtracting the increments due to inlet flow, lift, and the value at zero lift from the measured power on data. The data for the Internally Blown Flap (IBF) and the Upper Surface Blown (USB) systems (fig. 6a) show a linear variation with the lift increment due to blowing ΔC_{L_μ}. The dependence on wing sweep and flap span suggest that this side force increment may be carried on the flaps themselves. For these configurations, the increment of sideforce parameter due to blowing is given by:

$$\Delta C_{Y_{\beta_\mu}} = -0.038(1 - \cos \Lambda_{c/2}) \Delta C_{L_\mu} \qquad \text{for IBF configurations}$$

$$\Delta C_{Y_{\beta_\mu}} = -0.019(1 - \cos \Lambda_{c/2}) \Delta C_{L_\mu} \qquad \text{for USB configurations}$$

The data for the Externally Blown Flap (EBF) configurations (fig. 6b) show

$$\Delta C_{Y_{\beta_\mu}} = \left[-.038(1-\cos\Lambda_{c/2})\right] \Delta C_{L_\mu} \quad \text{for IBF}$$

$$\Delta C_{Y_{\beta_\mu}} = \left[-.019(1-\cos\Lambda_{c/2})\right] \Delta C_{L_\mu} \quad \text{for USB}$$

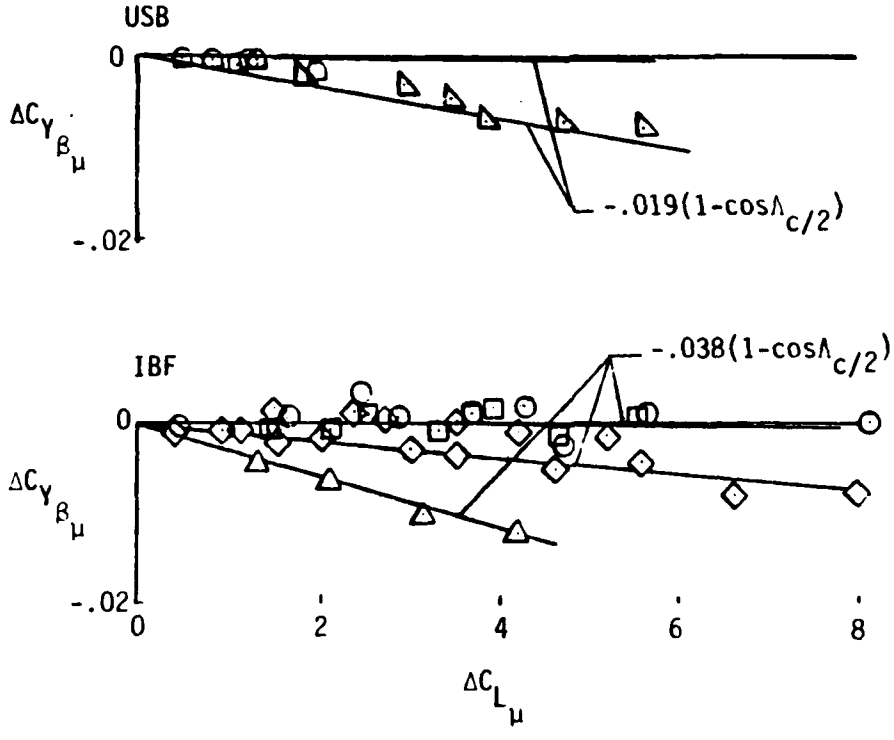

	$\Lambda_{c/2}$	A	b_j/b	Ref.	
□	3.0	9.4	.43	22	USB
△	24.2	7.0	.51	23	USB
○	3.5	9.24	1.0		IBF
□	3.5	6.26		29	IBF
◇	12.7	9.0			IBF
△	22.0	8.0		16	IBF

(a) IBF and USB Configuration

Figure 6 Side Force Due to Power.

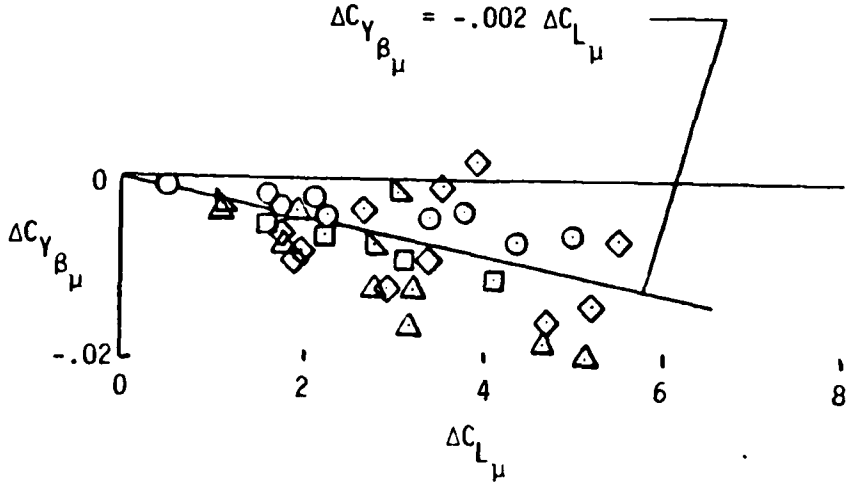

	$\Lambda_{c/2}$	A	Ref.
○	1.5	7.0	19
□	3	7.0	13
◇	22	7.23	11
▽	9.5	8.0	16
△	32	8.0	16

(b) EBF Configurations

Figure 6 Concluded

considerably more scatter than that for the IBF and USB configurations. Close examination of the data presented in figue 6b appears to show low values of $\Delta C_{Y_{\beta_\mu}}$ at the lowest sweep angles with the values increasing to a maximum at a sweep angle of 9.5 degrees and then reducing again at higher sweeps. A physical explanation for this type of variation could not be found and it was decided to treat the variations shown as scatter and draw a single line through the data. The increment in side force factor due to blowing is given by:

$$\Delta C_{Y_{\beta_\mu}} = -0.002\Delta C_{L_\mu} \qquad \text{for EBF configurations}$$

Directional Stability

As with the side force parameter, the directional stability parameter is made up of a zero lift term and terms due to power off lift, inlet flow and jet flap action. The directional stability parameter C_{n_β} can be expressed as:

$$C_{n_\beta} = C_{n_{\beta_D}} + \Delta C_{n_{\beta_o}} + \Delta C_{n_{\beta_i}} + \Delta C_{n_{\beta_\mu}}$$

where

$C_{n_{\beta_D}}$ is the DATCOM estimate from section 5.2.3.1 (including nacelles)

$\Delta C_{n_{\beta_o}}$ is the increment due to lift, power off

$\Delta C_{n_{\beta_i}}$ is the increment due to inlet flow

and

$\Delta C_{n_{\beta_\mu}}$ is the increment due to blowing.

The DATCOM estimate of C_{n_β} is based on the unstable moment of the fuselage (tail off) and is appropriate at zero angle of attack. The destabilizing effects of the nacelles should also be included in this estimate, particularly for EBF and USB configurations where the nacelles are large and generally located relatively far forward where the nacelle side force also adds significantly to the instability. Their yawing moment contribution (treated as small fuselages in the DATCOM method) plus their side force contribution multiplied by the appropriate arm should be added to the DATCOM estimate of the fuselage contribution in estimating $C_{n_{\beta_D}}$

Effect of Lift

As with the side force, Toll and Queijo in reference 5 developed expressions for the yawing moment of swept wings at high lift coefficients. The resulting expressions are included in the DATCOM in section 5.1.3.1 but are seldom applied because this contribution is a function of $C_L{}^2$ and at lift coefficients appropriate to cruise configurations, the contribution is negligible. With flaps deflected, however, power off lift coefficients over 3 can be reached and this term should be significant.

Figure 7 presents the increments of the directional stability parameter C_{n_β} as a function of lift coefficient squared for a variety of configurations. This increment, which is stabilizing, was obtained by subtracting the value of C_{n_β} at zero lift (using faired data) from the data at lift. Figure 7 shows relatively good correlation and, as predicted by Toll and Queijo, a dependence on wing sweep. The values obtained, however, are about 40 percent of those predicted by Toll and Queijo in reference 5. Toll and Queijo also predicted an increase in this increment with decreasing aspect ratio particularly at low aspect ratios. The aspect ratio range

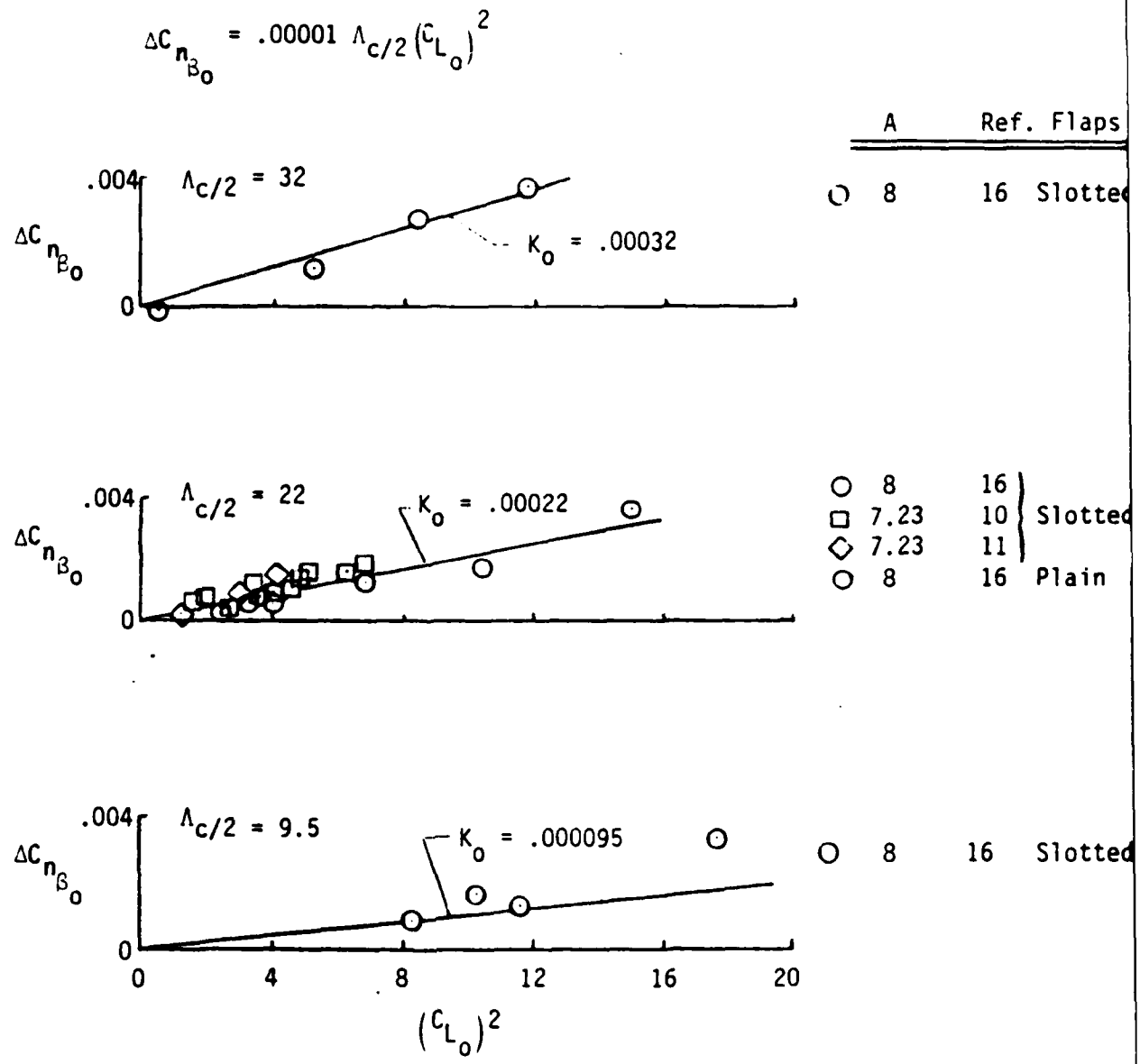

Figure 7 Effect of Flaps on C_{n_β}; Power Off.

covered in the available data is too limited to confirm this trend but it should be kept in mind if there are attempts to apply the present method to low aspect ratio configurations.

For the present method, the increment of the directional stability parameter due to lift is given by:

$$\Delta C_{n_{\beta_o}} = 0.00001 \Lambda_{c/2} (C_{L_o})^2$$

Effect of Inlet Flow

The effects of power on the directional stability parameter C_{n_β} (tail off) arise from two sources: the effects of inlet flow and the effects of blowing or jet flap action.

The inlet contribution to yawing moment results from turning the flow into the inlets and is destabilizing for configurations with the inlets ahead of the moment reference point as is typical of powered lift STOL configurations. The yawing moment is simply the side force due to inlet flow multiplied by the distance from the moment reference point to the inlet face.

The inlet contribution to the directional stability parameter C_n is given by:

$$\Delta C_{n_{\beta_i}} = \Delta C_{Y_{\beta_i}} \left(\frac{x_i}{b} \cos \alpha - \frac{z_i}{b} \sin \alpha \right)$$

Effect of Blowing

The effects of jet flap action are presented in figures 8 and 9 and were obtained by subtracting the increments due to inlet flow, lift, and

the value at zero lift from the measured power on data. The increment of the directional stability parameter due to blowing appears to be proportional to the square root of the lift coefficient due to blowing and to be dependent on wing geometry and on the type of jet flap system used.

As with side force, there is considerable scatter in the data and there are indications that the yawing moment is dependent on how well the flap system is working. An extreme example is shown in figure 8b where a double slotted flap system and a triple slotted flap system, both deflected 60 degrees on the same wing produce almost the same lift but greatly different yawing moments increments. Apparently, the double slotted flap system is being worked near the limit of its capability and probably encountering some flow separation which causes the large yawing moments. (Data are available only at an angle of attack of 10 degrees and at only one blowing coefficient for each flap system.) The lift and drag data were analyzed in hopes of finding characteristics that would explain and correlate with these differences in yawing moments. While the double slotted configuration was operating closer to the lift coefficient at which the drag begins to rise rapidly there was very little difference in the lift curve slope, lift-drag ratio or rate of change of drag with lift at the actual lift coefficients at which the two flap systems were operating. Apparently, yawing moment data is more sensitive to incipient flow separation (probably because it is dependent on where separation starts on the wing span) than the lift and drag data. In general, emphasis was placed on the data from the lower flap deflections wherever possible in making correlations used in developing the methods in this study.

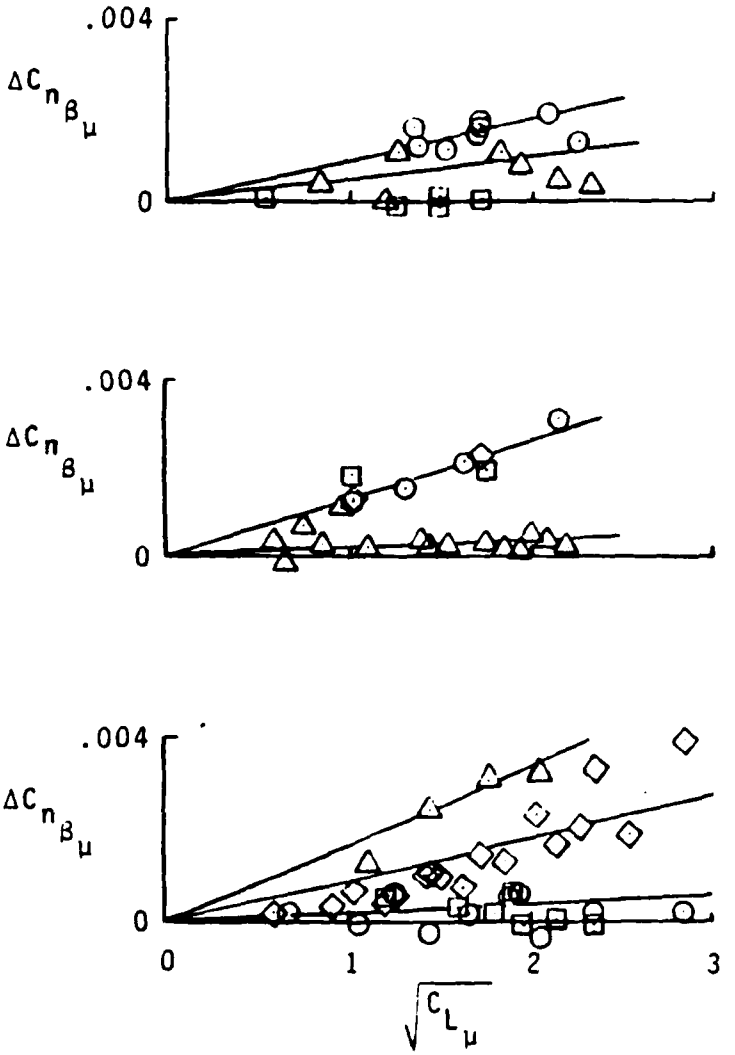

	$\Lambda_{c/2}$	A	b_j/b	Ref
○	22	7.23	.35	10
□	3	7.0		13
△	24.2	7.0	.51	23
○	9.5	9.0	.58	16
□	22			
◇	32			
△	3.0	7.0	.54	19
○	3.5	9.2	1.0	29
□	3.5	6.2		
◇	12.7	9.0		
△	22	8.0		16

(a) Basic data used

Figure 8 Yawing Moment Increments Due to Power.

	δ_f	Type of Flaps
○	30	Double Slotted
□	60	Double Slotted
◇	60	Triple slotted

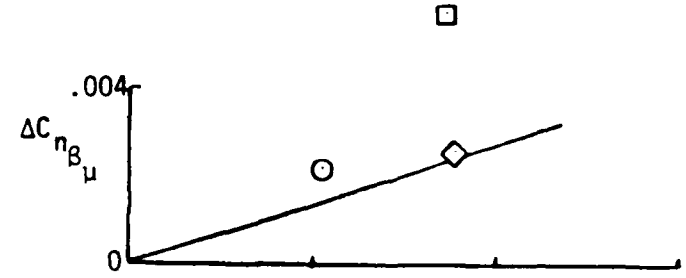

$\Lambda_{c/2}$ = 22
A = 7.14
b_j/b = .581

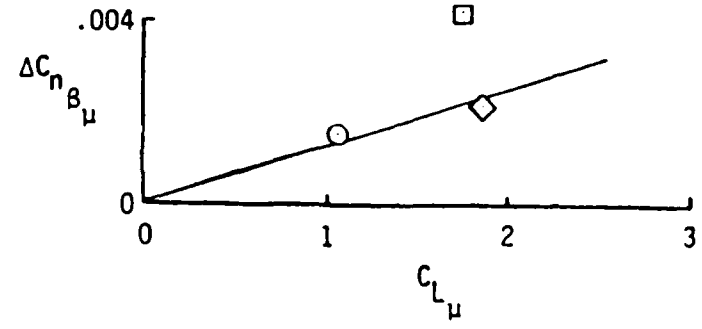

$\Lambda_{c/2}$ = 22
A = 9.52
b_j/b = .581

(b) Effect of Flap Configuration, Ref. 16

Figure 8 Concluded

$$\Delta C_{n_{\beta_\mu}} = K_{n_\mu} \Lambda_{c/2} \sqrt{\Delta C_{L_\mu}} \sqrt{b_j/b}$$

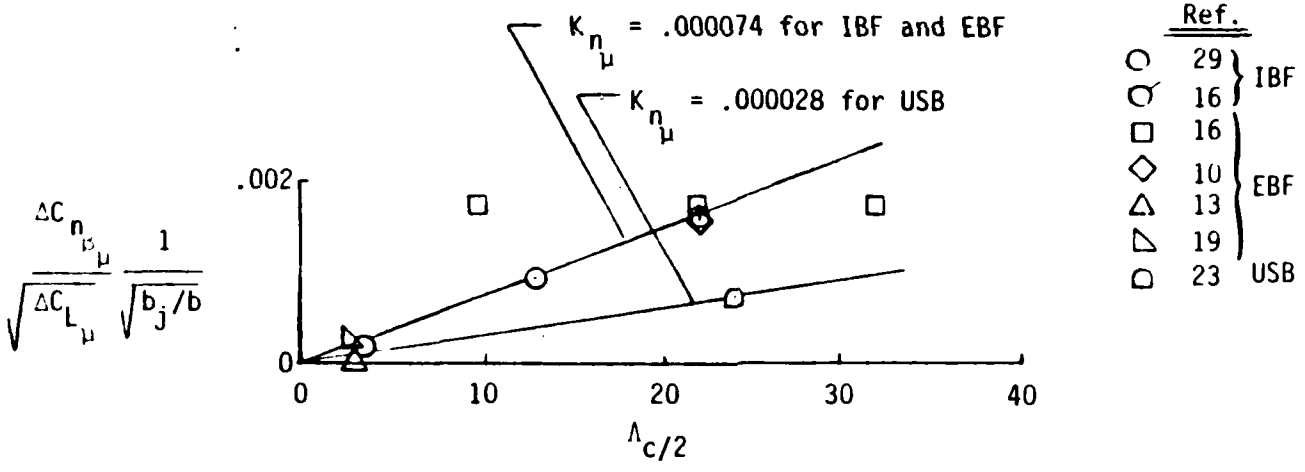

Figure 9 Method for Estimating Yawing Moment Increment Due to Blowing

The increment of the directional stability parameter due to blowing $\Delta C_{n_{\beta_\mu}}$ is correlated with the wing sweep and flap span in figure 9. For essentially unswept wings, all jet flap concepts show essentially zero effect of power on the directional stability parameter $\Delta C_{n_{\beta_\mu}}$. The IFB system shows a linear increase with wing sweep but the data from reference 16 implies an unusual variation for the EBF systems; a rapid increase with sweep to about 9 or 10 degrees sweep followed by a constant level at higher sweep angles. (The data of reference 16 were presented only at an angle of attack of 10 degrees and for only one blowing coefficient.) A logical physical explanation for this trend could not be found and, therefore, the linear variation with sweep identical to that for the IBF system has been adopted. A linear variation of lower slope was also adopted for the USB system.

For the present method, the increment of the directional stability parameter due to power is given by:

$$\Delta C_{n_{\beta_\mu}} = -0.000074 \Lambda_{c/2} \sqrt{\frac{b_j}{b}} \sqrt{\Delta C_{L_\mu}} \qquad \text{for IBF and EBF}$$

$$\Delta C_{n_{\beta_\mu}} = -0.000028 \Lambda_{c/2} \sqrt{\frac{b_j}{b}} \sqrt{\Delta C_{L_\mu}} \qquad \text{for USB}$$

Dihedral Effect

Five terms are used in estimating the effective dihedral parameter C_{ℓ_β}:

$$C_{\ell_\beta} = C_{\ell_{\beta_o}} + \left(\frac{C_{\ell_\beta}}{C_L}\right)_D C_{L_o} + \Delta C_{\ell_{\beta_f}} + \Delta C_{\ell_{\beta_i}} + \Delta C_{\ell_{\beta_\mu}}$$

where $C_{\ell_{\beta_o}}$ is the DATCOM estimate of C_{ℓ_β} at zero lift from Section 5.2.2.1

$\left(\frac{C_{\ell_\beta}}{C_L}\right)_D$ is the DATCOM estimate of the effect of lift coefficient on C_{ℓ_β} from Section 5.2.2.1

$\Delta C_{\ell_{\beta_f}}$ is the increment due to flaps

$\Delta C_{\ell_{\beta_i}}$ is the increment due to inlet flow

and

$\Delta C_{\ell_{\beta_\mu}}$ is the increment due to blowing.

The DATCOM method for estimating the effective dihedral parameter C_{ℓ_β} consists of several terms that can be collected into two groups: those due to geometric dihedral, wing height and wing twist that are independent of lift coefficient and lumped here as $C_{\ell_{\beta_o}}$ and those that are a function of lift coefficient lumped here as $(C_{L_\beta}/C_L)_D$. The DATCOM method for estimating the terms that are a function of lift coefficient is based on the work of Polhamus and Sleeman in reference 6.

Effect of Lift

The method of reference 6 is based largely on the difference in the lifting ability of the windward and leeward wing panels when the configuration is sideslipping. With an unswept wing, the windward tip begins to act

like a leading edge and the leeward tip a trailing edge when sideslipping producing a positive dihedral effect (negative C_{ℓ_β}). This effect is increased with a swept wing because the increase in effective aspect ratio and decrease in sweep of the windward panel increases its lift curve slope relative to the leeward panel which experiences a decrease in lift-curve slope because of the increase in sweep and decrease in aspect ratio. These differential changes in panel geometry would also be expected to increase the flap and blowing effectiveness on the windward panel and decrease them on the leeward panel and cause the dihedral effect to increase (more negative C_{ℓ_β}) with both flap deflection and blowing. This hypothesis is only partially supported by the data (see for example figures 2 and 4). For most configurations, flap deflection and blowing produce a positive increment in C_{ℓ_β} (negative dihedral effect). Apparently, there are factors at work that cause the total lift to shift slightly to leeward.

The effect of flap deflection on dihedral effect is shown in figure 10. These data were obtained by subtracting the effective dihedral parameter estimated by the DATCOM method $[C_{\ell_{\beta_o}} + (C_{\ell_\beta}/C_L)C_{L_o}]$ from the measured data with the flaps deflected (power off). The large amount of scatter at the highest values of the correlating parameter is believed to be due to flow separation. These data points are from flap deflections of 60 degrees on a wing at 10 degrees angle of attack. The data and the correlation in figure 10 indicate that flap deflection causes a negative dihedral effect (positive values of $\Delta C_{\ell_{\beta_f}}$) for wings with geometric dihedral but have no effect on the effective dihedral when the geometric dihedral is zero. A positive shift in C_{ℓ_β} can be explained as an effective shift of the total

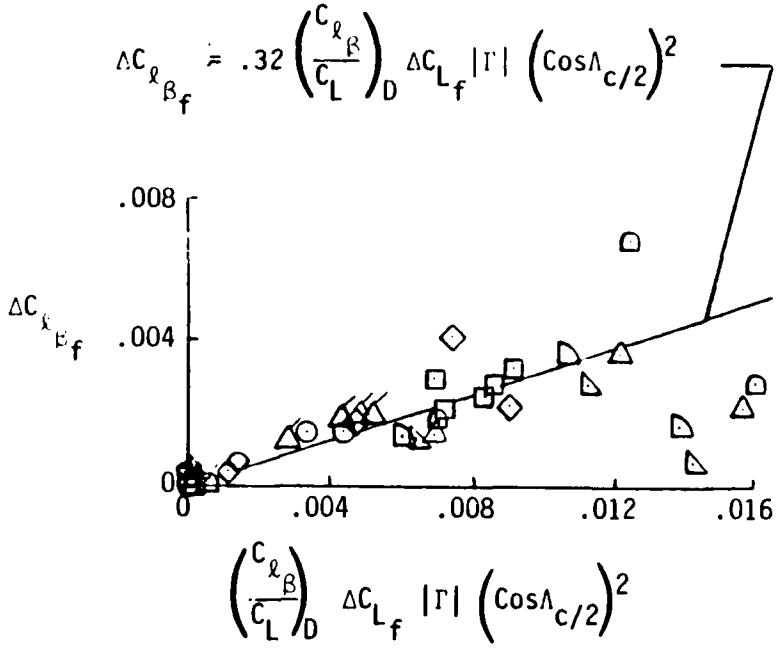

	$\Lambda_{c/2}$	A	Γ	Ref.	
○	22	7.75	-3.5	9	Slotted Flaps
□	22	7.23		10 & 11	
◇	9.5	8.0			
△	22				
▱	32			16	
▱	22	9.52			
□	22	7.14			
◇	3.0	7.0	+2.8	13	
Q	22	7.27	0	18	
□	2	7.0	0	19	Plain Flaps
◇	3	9.4	0	20	
△	22	8.0	-3.5	16	
◪	3.5	9.2	-1		
◪	3.5	9.2	+4	29	
◫	12.7	9.0	-1		
◇	43	4.0	0	7	

Figure 10 Effect of Flaps on C_{ℓ_β} ; Power Off.

lift toward the leeward and could be caused by the corresponding shift in total wing-flap vortex system. There appears to be no physical explanation, however, for why this should occur for wings with geometric dihedral and not for wings with zero dihedral. Nevertheless, the evidence is so strong both in the data used in figure 10 and in other references (refs. 4, 17, 26, and 27 clearly show the large negative values of C_{ℓ_β} associated with zero dihedral but could not be included in figure 10 because tail off data were not presented) that geometric dihedral is included in the correlating parameter.

One problem encountered in developing the correlation shown in figure 10 was that of determining the appropriate value of flap lift increment ΔC_{L_f} to use. Most configurations designed to achieve high power on lift coefficients are fitted with a large chord highly deflected leading edge slat or flap. Under power off conditions, this leading edge device is usually stalled on the lower surface at negative (and often at zero) angles of attack. On the other hand, with the high flap deflections often used, wing-flap separation often occurs at angles of attack of 10 degrees and higher in the power off condition. Careful inspection of the lift curves is required in determining the true lift increment due to flap deflection.

For the present method, the increment of the effective dihedral parameter due to flap lift is given by:

$$\Delta C_{\ell_{\beta_f}} = 0.32 \left(\frac{C_{\ell_\beta}}{C_L} \right)_n \Delta C_{L_f} \left| \Gamma \right| (\cos \Lambda_{c/2})^2$$

Effect of Inlet Flow

As with directional stability, the effects of power on the effective dihedral (tail off) arise from two sources: the effects of inlet flow and the effects of blowing or jet flap action.

The inlet contribution to rolling moment is generally small because the vertical distance from the moment reference point is usually small but can be easily included and is given by:

$$\Delta C_{\ell_{\beta_i}} = \Delta C_{Y_{\beta_i}} \left(\frac{z_i}{b} \cos \alpha + \frac{x_i}{b} \sin \alpha\right)$$

Effect of Blowing

The effects of jet flap action, or blowing, are presented in figures 11 and 12 and were obtained by subtracting the DATCOM estimate, the increment due to flap deflection, and the increment due to inlet flow from the power on data.

For EBF and USB configurations, as shown by representative examples in figure 11, there are effects of wing planform but there is no discernible effect of flap deflection or angle of attack. However, for the IBF configurations of reference 29 (fig. 12), the increment of the effective dihedral parameter due to power $\Delta C_{\ell_{\beta_\mu}}$ clearly increases with both angle of attack and flap deflection. The increase appears to be related to the angle, relative to the free stream, at which the jet leaves the trailing edge of the flap ($\theta + \alpha$). In estimating this angle, the jet sheet deflection angle, θ, is (for the IBF configurations) taken as the flap upper surface trailing edge angle.

The data for both EBF and IBF configurations also show effects of aspect ratio, sweep, and geometric dihedral on the effective dihedral parameter due to power $\Delta C_{\ell_{\beta_\mu}}$. The increment of the effective dihedral parameter due to power can be expressed as:

$$\Delta C_{\ell_{\beta_\mu}} = (K_{\ell_\Lambda} + K_{\ell_A} + K_{\ell_\Gamma} + K_{\ell_\theta})\Delta C_{L_\mu}$$

The effects of aspect ratio and geometric dihedral were isolated using primarily the data of references 16 and 29 as shown in figure 13. These appear to be equally applicable to both EBF and IBF systems. The effects of jet sheet deflection were also obtained from the data of references 16 and 29 and are shown in figure 14. The effect of jet sheet deflection is proportional to the square of the deflection angle and applies to IBF systems only.

The effect of sweep on the increment of the effective dihedral parameter due to blowing was obtained by subtracting the effects of aspect ratio, dihedral and jet sheet deflection, as estimated by the correlations shown in figures 13 and 14 from the total increments due to blowing (such as shown in figures 11 and 12). The values of K_{ℓ_Λ} thus obtained are presented in figure 15. A negative value of K_{ℓ_Λ} is shown for IBF, EBF, and USB configurations at zero sweep because the positive effect is included in the factor for aspect ratio. The data shows the expected increase in positive dihedral effect (negative values of K_{ℓ_Λ}) with increasing sweep. The EBF and USB configurations show less negative values, probably because of the distance between the jet nozzle and the flap system in these configurations. That is, because the jet exhaust is ahead of the flap system it can

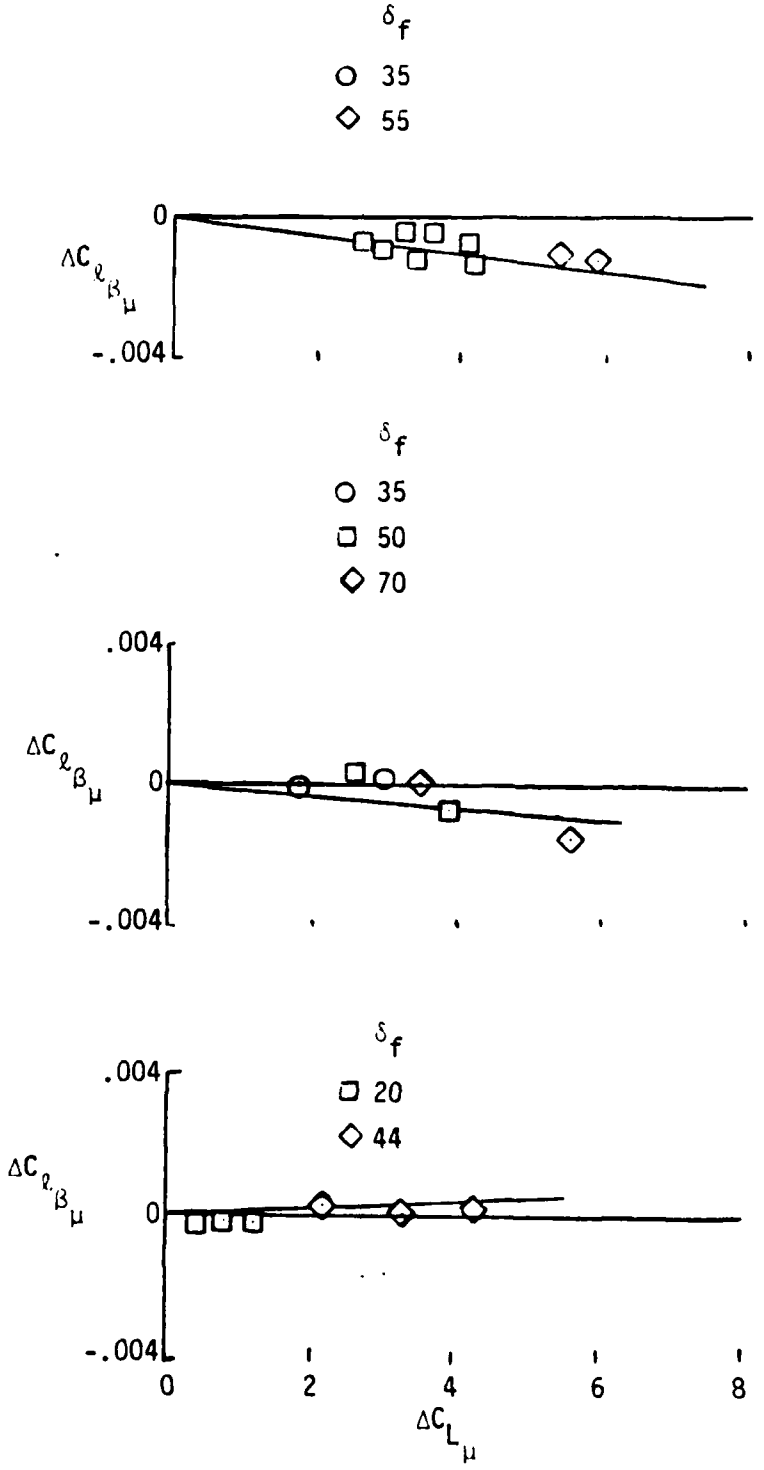

Figure 11 Increment of C_{ℓ_β} Due to Power. Selected EBF and USB Configurat

Est.	Exp.	δ_f	α	$(\theta + \alpha)$
———	○	0	0	20
— — —	□	30	0	50
— · —	◇	30	20	70

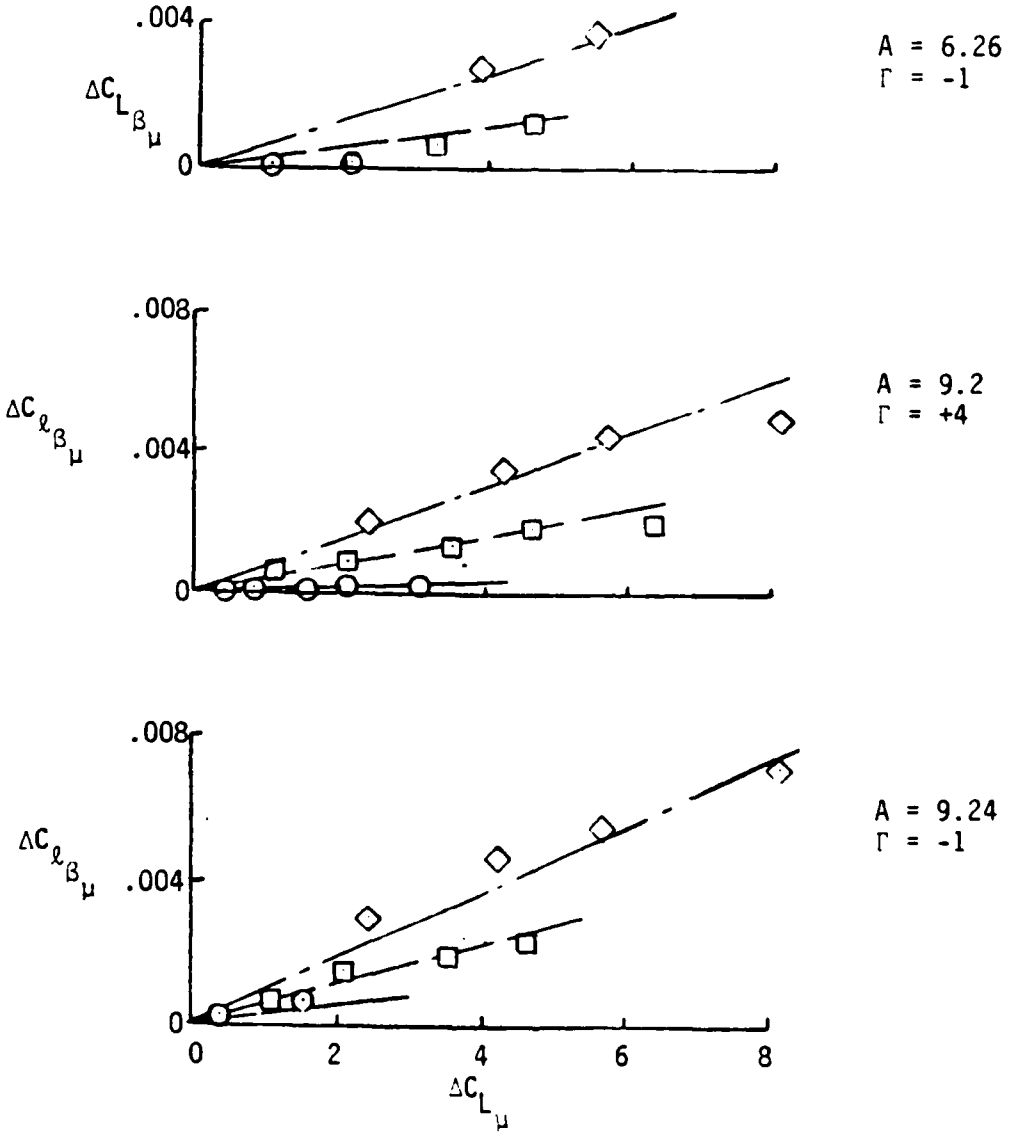

Figure 12 Increment of C_{ℓ_β} Due to Power, IBF Configurations. -Ref. 29

$$\Delta C_{\ell_{\beta_\mu}} = \left(K_{\ell_\Lambda} + K_{\ell_A} + K_{\ell_\Gamma} + K_{\ell_{(\theta+\alpha)}}\right) \Delta C_{L_\mu}$$

	$\Lambda_{c/2}$	Γ	Ref.	
○	3.5	-1	29	IBF
□	22	-3.5	16	EBF

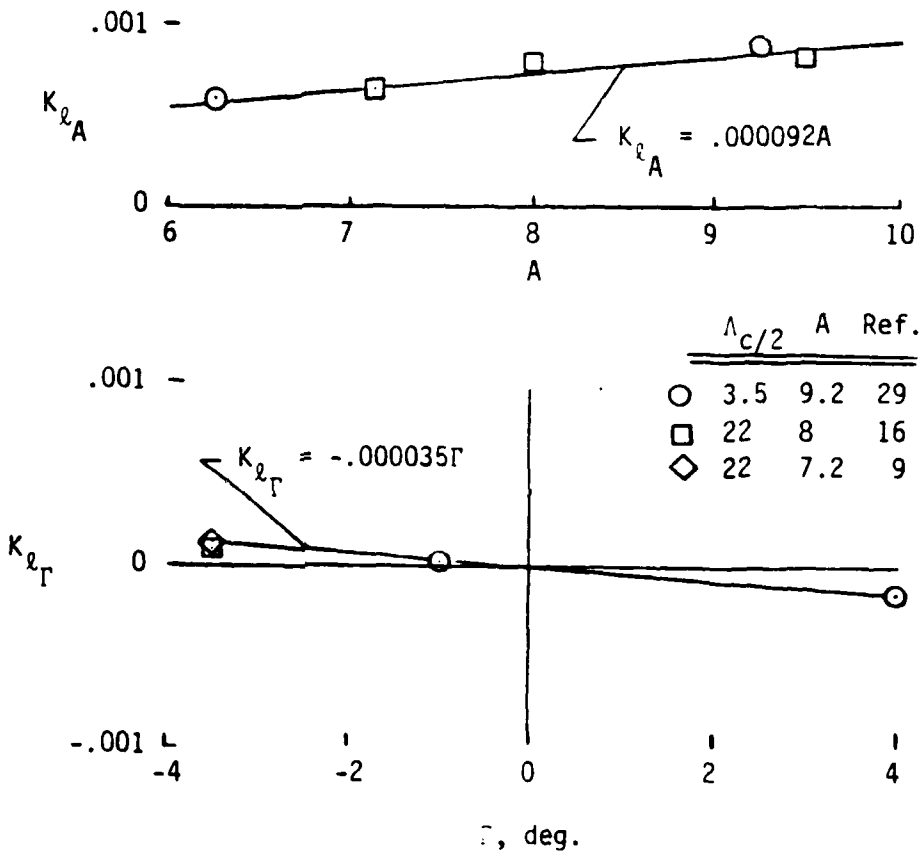

Figure 13 Effect of Dihedral and Aspect Ratio on K_ℓ.

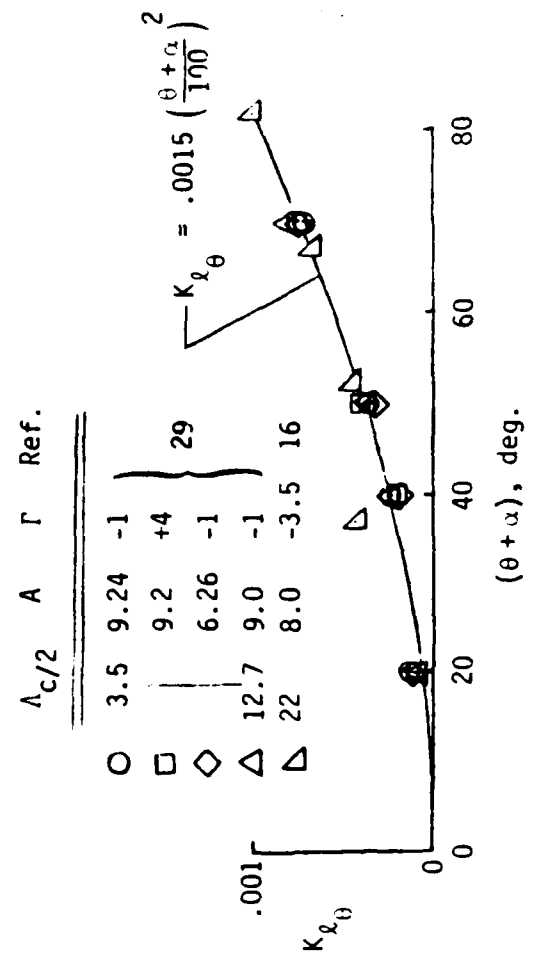

Figure 14 Effect of Jet Sheet Deflection on K_{ℓ_θ}. IBF Configurations Only.

$$\Delta C_{\ell_{\beta_\mu}} = \left[K_{\ell_\Lambda} + .000092A - .000035\Gamma + K_\theta\left(\frac{\theta+\alpha}{100}\right)^2\right]\Delta C_{L_\mu}$$

For IBF $K_{\ell_\Lambda} = -.00065-.0195(1-\cos\Lambda_{c/2})$ and $K_\theta = .0015$

For EBF & USB $K_{\ell_\Lambda} = -.00045-.009(1-\cos\Lambda_{c/2})$ and $K_\theta = 0$

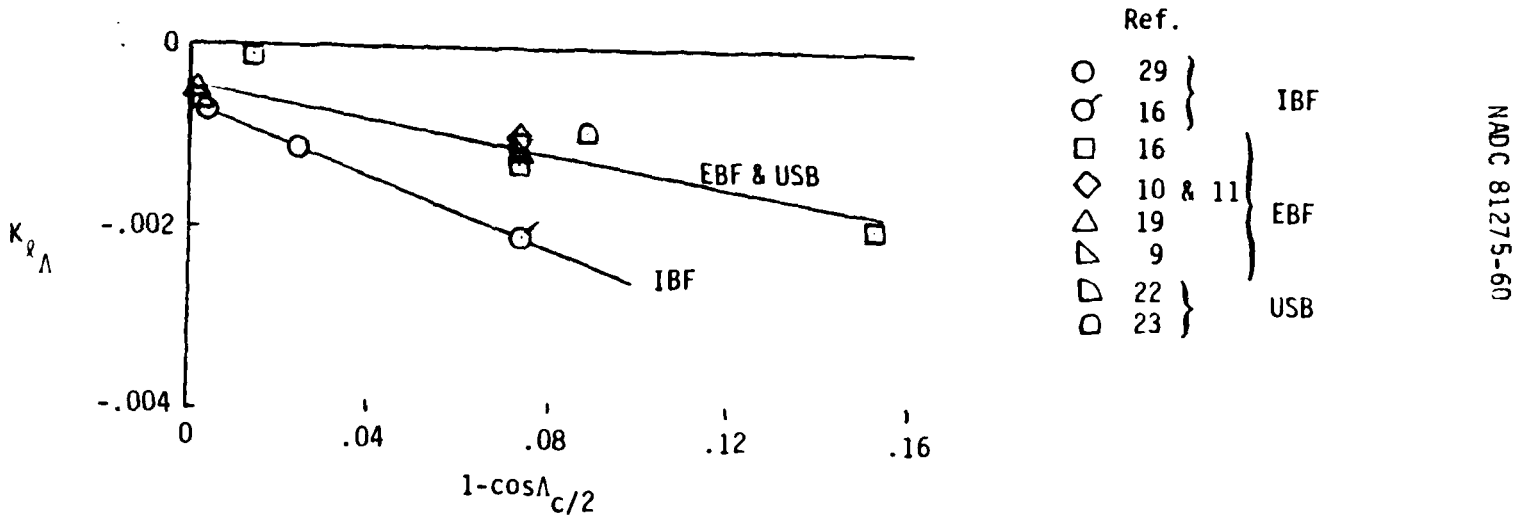

Figure 15 Effect of Sweep on K_ℓ and Presentation of Method for Estimating the Increment of C_{ℓ_β} Due to Power.

be deflected slightly to leeward by the free stream before reaching the flap system, thus, shifting the flap lift to leeward and producing a positive increment in $\Delta C_{\ell_{\beta_\mu}}$ (negative dihedral effect).

For the present method, the increment of the effective dihedral parameter due to blowing is given by:

$$\Delta C_{\ell_{\beta_\mu}} = [K_{\ell_\Lambda} + 0.000092A - 0.000035\Gamma + K_\theta(\frac{\theta + \alpha}{100})^2]\Delta C_{L_\mu}$$

where

$K_{\ell_\Lambda} = -0.00065 - 0.0195(1 - \cos \Lambda_{c/2})$ for IBF configurations

$K_{\ell_\Lambda} = -0.00045 - 0.009\ (1 - \cos \Lambda_{c/2})$ for EBF and USB configurations

and

$K_\theta = 0.0015$ for IBF configurations

$K_\theta = 0$ for EBF and USB configurations

Tail Contribution

Examination of the data shows that, in general, the contribution of the tail to both side force and directional stability increases significantly with both flap deflection and power. This increase in tail contribution results from a favorable sidewash induced at the tail. Examination of rudder effectiveness data, vertical tail effectiveness data obtained by incidence variation, and limited dynamic pressure surveys at the vertical tail shows that, in the angle of attack range where the wing-flap system is

not stalled, the dynamic pressure at the vertical tail does not vary by more than about 5 percent from the free stream value.

Figure 16, taken from reference 13, gives some indication of the flow behind an EBF configuration at moderate flap deflections. In this case, smoke was introduced to try to show the vortex flow originating from the outboard end of the flap.

The total flow field behind a powered lift configuration is complex as partially depicted in figure 17. In addition to the vortices from the flap tips, there are wing tip vortices and vortices originating at the outboard end of the powered lift portion of the flaps as well as a pair of vortices from the wing root rotating in the opposite direction to the others. Not shown are the cross flow around the fuselage and the body vortices arising from the side force carried on the fuselage. The system does not stay as orderly as depicted in figure 17 because the vortices interact and the predominant vortex, although itself moved by the others, tends to move the others about itself. Surveys a relatively short distance behind a wing have shown the remnants of the wing tip vortex can be moved almost to the centerline and the inboard vortex moved almost out to the wing tip. Nevertheless, there is a strong general vortex flow behind the wing-flap system and a tail placed asymmetrically in that flow field, as occurs with sideslip, will experience a sidewash that is favorable for the types of configurations being considered.

Because of the complexity of the flow field behind a powered lift wing and the interaction between the vortices, it is not feasible to attempt to estimate the sidewash by trying to construct a vortex system such as is

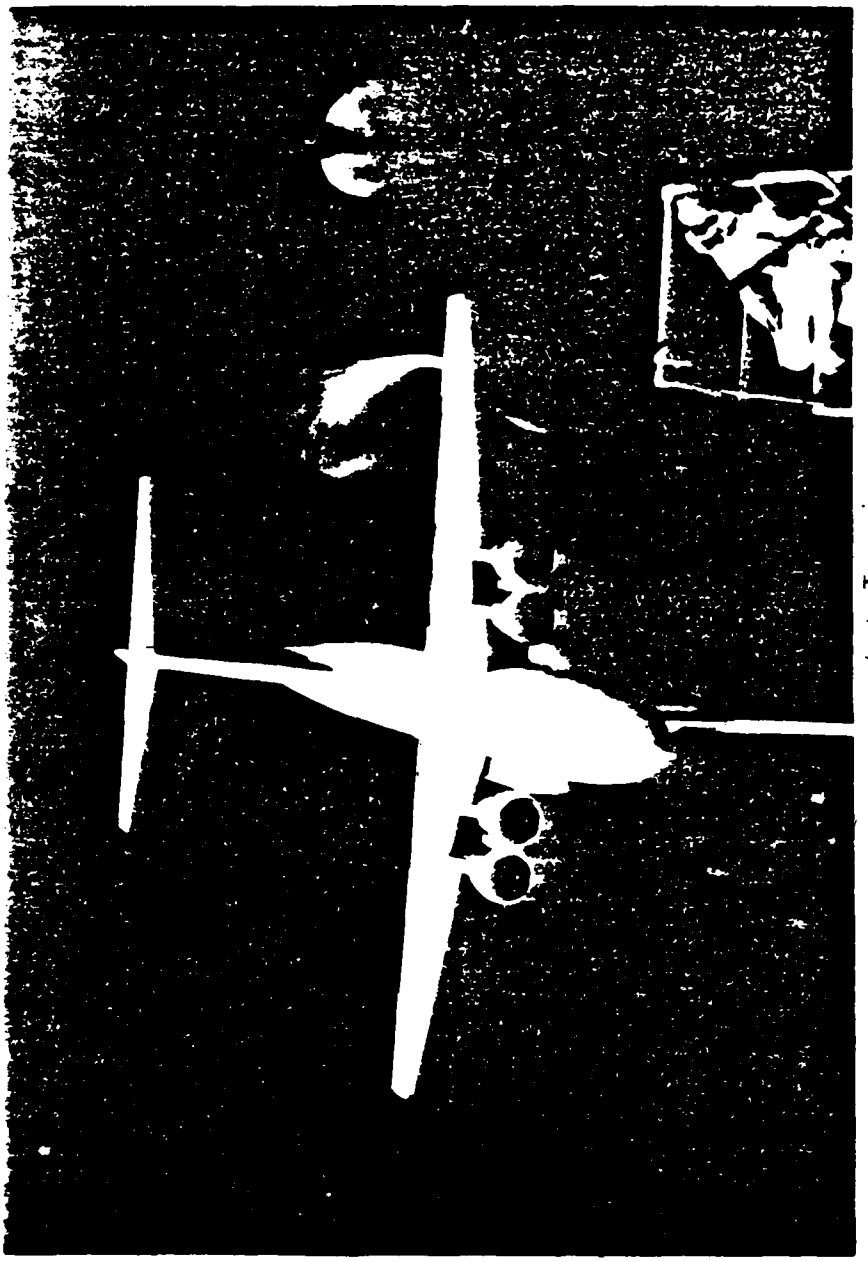

(a) Top view.

Figure 16 Flow in the Wake of the Model of Reference 13, Photo Courtesy of NASA.

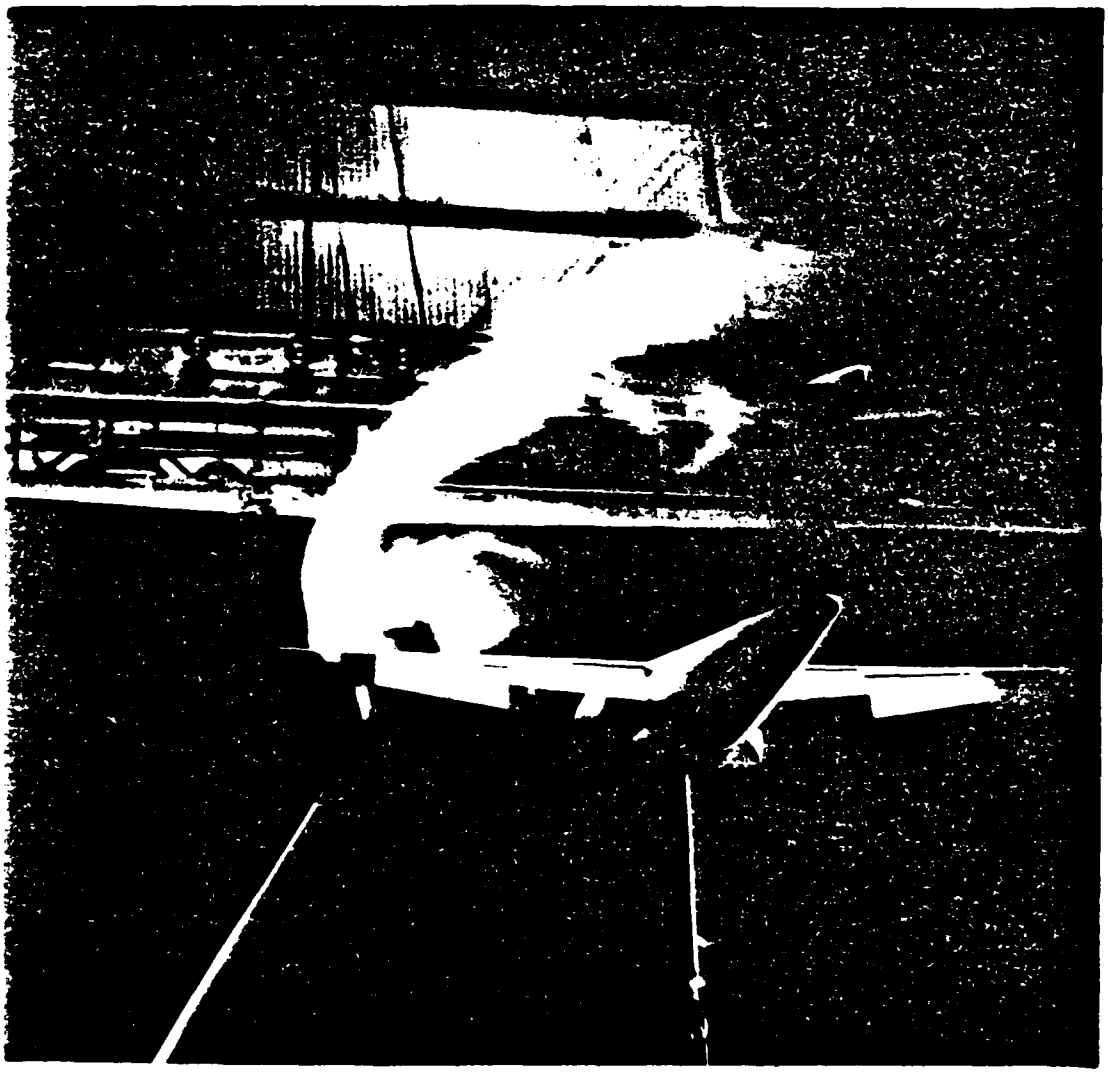

(b) Three-quarter rear view.

Figure 16 Concluded

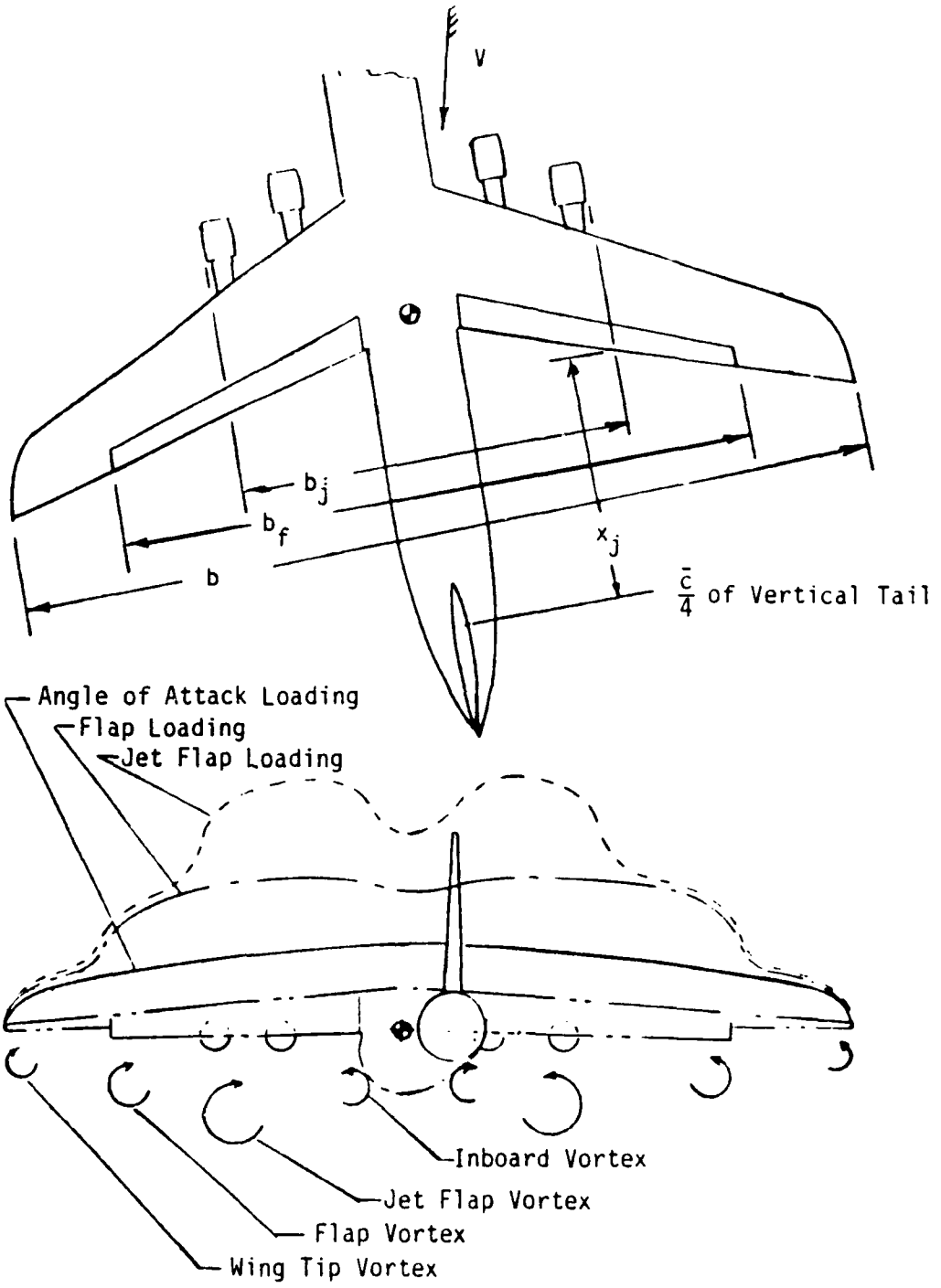

Figure 17 Schematic of Wing Span Load Distribution and Wake System.

shown in figure 17. In the present study, the effective sidewash was determined from the measured tail contributions.

Convair, in reference 15, made measurements of the sidewash at the position of the vertical tail for a 60-degree flap at several angles of attack and power conditions. They presented the data as three curves as a function of momentum coefficient but, when replotted against the lift coefficient at which the wing was operating, the correlation shown in figure 18 was obtained. The correlation shown is better than expected because this is a full span flap system and, in the power off condition (flagged symbols on figure 18), the predominant vortices would be arising from the wing tip. At the highest lift coefficients, most of the lift is generated by jet flap action, the primary vortices should be further inboard and the sidewash per unit lift coefficient should be stronger because the lift is carried on a shorter span. The agreement shown indicates that there are compensating factors at work.

In this study the sidewash factor K_σ for each configuration for which adequate data were available was determined from the yawing moment data rather than the sideforce data because the yawing moment data is usually more accurate. The sidewash factor was determined from the directional stability data by:

$$K_\sigma = \frac{\left(\Delta C_{n_{\beta_t}}\right)_m}{\left(\Delta C_{n_{\beta_t}}\right)_D} - 1$$

where

$\Delta C_{n_{\beta_t}}{}_m$ is the measured contribution of the tail to the directional stability obtained by subtracting the tail off directional stability data from the complete model data.

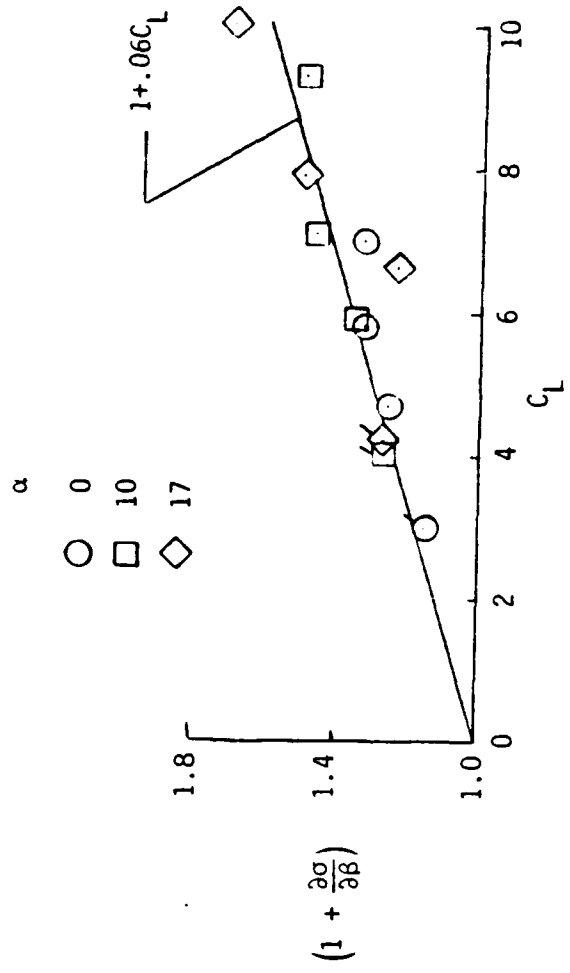

Figure 18 Sidewash Measured in Reference 15 for the A = 8.0, $\Lambda_{c/2}$ = 22 Wing with Triple Slotted Flaps Deflected 60°.

and $\left(\Delta C_{n_{\beta_t}}\right)_D$ is the DATCOM estimate of the tail contribution from section 5.3.1.1.

Typical data for three configurations are presented in figure 19. The data from reference 16 are for the same configuration for which the sidewash measurements were made in reference 15 and are presented in figure 18. There is considerable scatter in the data but the average sidewash factor is in agreement with that presented in figure 18. The data from references 10 and 11 were measured on the same model tested at two different times.

It is interesting to compare the sidewash data from references 10 and 11 with the sidewash data from reference 9. These models had identical fuselage tail configurations. The model of references 10 and 11 has the shortest jet flap span (as defined in figure 17) and the highest sidewash factor. The model of reference 9 has a greater jet flap span and a lower sidewash factor. Going a step further, the model of reference 16 has the largest jet flap span and the lowest sidewash factor. This trend appears to be logical at least for the high power lift conditions where most of the lift is being generated by the jet flap action. The vortex strength and, therefore, the sidewash should be inversely proportional to the span over which the lift is carried and, at the high power conditions, this should be the effective span of the jet flap system. The effective span of the jet flap system cannot be determined; therefore, the span covered by the nacelles as shown in figure 17 is used here as a measure of the jet flap span in the present method.

The sidewash would also be expected to decay with distance downstream from the point of origin of the vortex system generating the sidewash. The

$$K_\sigma = \frac{\left(\Delta C_{n_{\beta_t}}\right)_m}{\left(\Delta C_{n_{\beta_t}}\right)_D} - 1$$

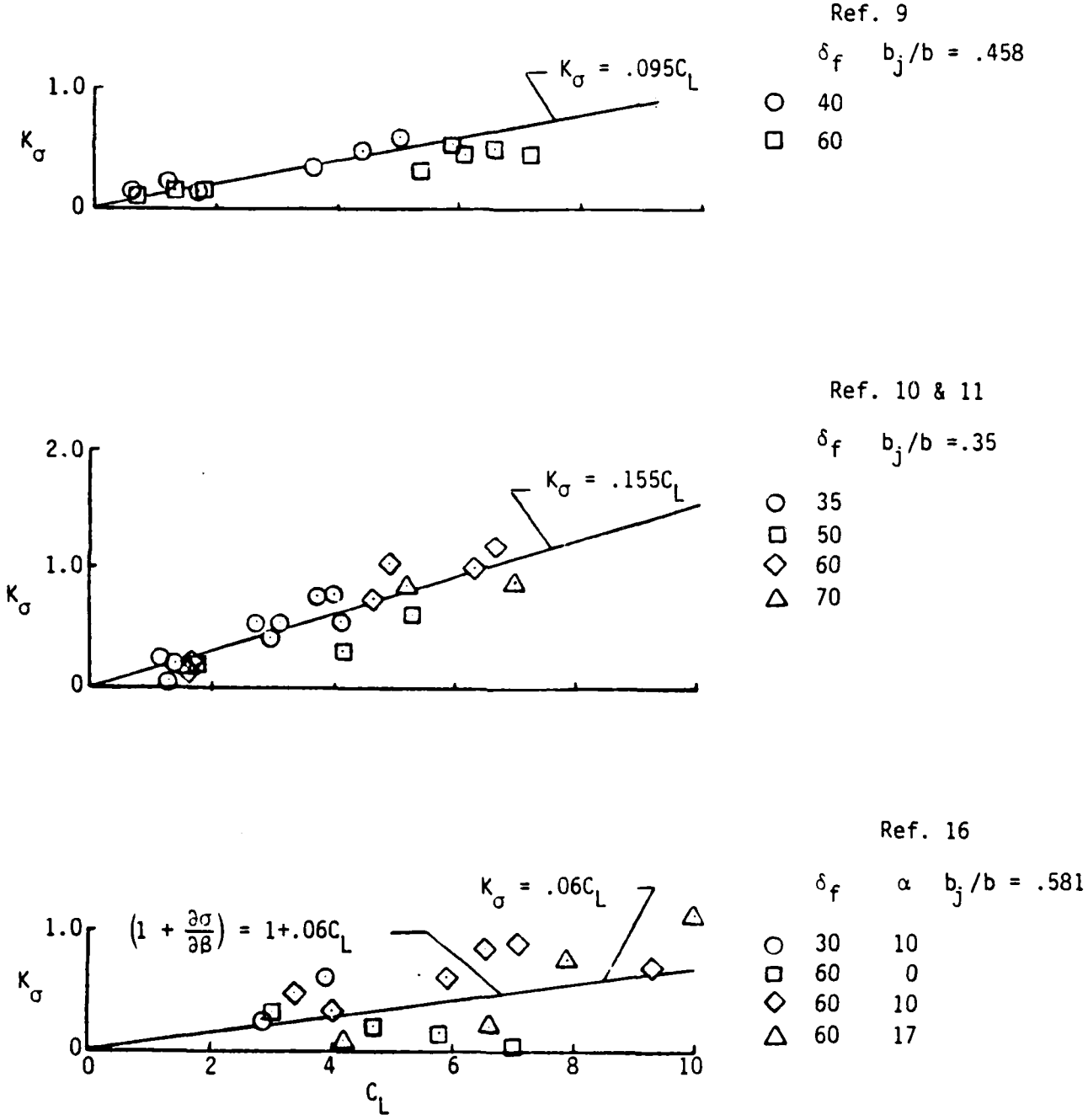

Figure 19 Effective Sidewash Factors for Several Configurations Determined from Yawing Moment Data.

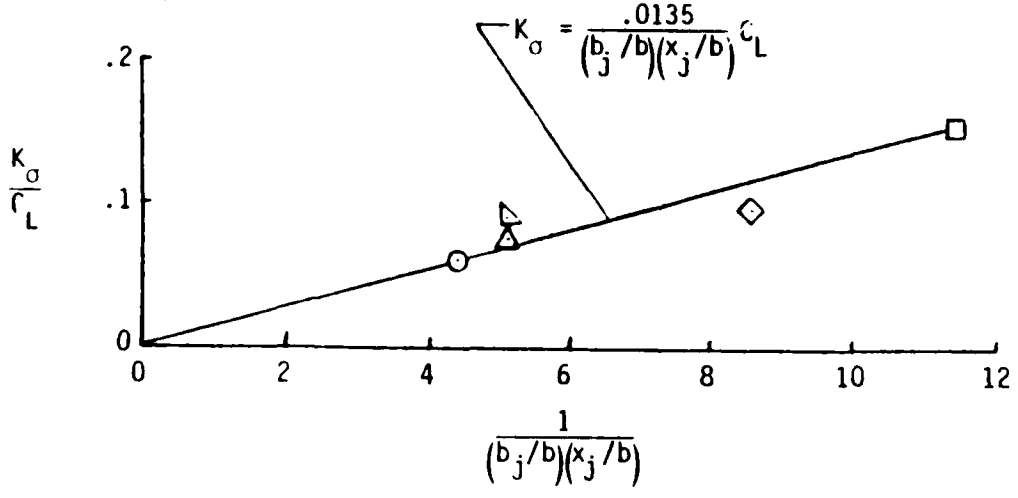

	$\Lambda_{c/2}$	b_j/b	x_j/b	Ref.
○	22	.581	.374	16
□	22	.35	.25	10 & 11
◇	22	.458	.238	9
△	2	.541	.359	19
◺	3	.443	.445	13

Figure 20 Correlation of Sidewash Factor with Jet Flap Span and Tail Length for Several EBF Configurations.

tail length as defined in figure 17 is used to represent this distance. The sidewash is shown to correlate reasonably well with the inverse of the product of jet flap span and this tail length as shown in figure 20. These data are for EBF configurations. Similar data are not available for IBF and USB configurations, but these would be expected to behave similarly and the correlation shown in figure 20 is, therefore, used for those configurations as well.

For the present method, the sidewash at the tail is given by:

$$K_\sigma = \frac{0.0135}{\frac{b_j}{b}\,\frac{x_j}{b}}\, C_L$$

And the contributions of the tail to side force, directional stability and dihedral effect are given by:

$$\Delta C_{Y_{\beta_t}} = \left(\Delta C_{Y_{\beta_t}}\right)_D (1 + K_\sigma)$$

$$\Delta C_{n_{\beta_t}} = \left(\Delta C_{Y_{\beta_t}}\right)_D (1 + K_\sigma)\left(\frac{x_t}{b}\cos\alpha + \frac{z_t}{b}\sin\alpha\right)$$

$$\Delta C_{\ell_{\beta_t}} = \left(\Delta C_{Y_{\beta_t}}\right)_D (1 + K_\sigma)\left(\frac{z_t}{b}\cos\alpha - \frac{x_t}{b}\sin\alpha\right)$$

COMPARISON OF ESTIMATES WITH EXPERIMENTAL DATA

Comparison of the estimates made with the present method for two of the configurations on which the method is based are presented in figures 2 and 4. Additional comparisons, most with data from configurations not used in developing the method are presented in this section.

EBF Configurations

The data of references 10 and 11 were taken on the same model tested at two different times. Estimates for the tail off configuration are compared with the data of reference 10 in figure 2. Both tail off and tail on estimates are compared with the data from reference 11 in figure 22.

Tail off and tail on estimates for the YC-15 EBF configuration are compared with data from model tests (ref. 19) in figure 24.

Additional comparisons for the model of reference 18 (also presented in figure 4) are presented in figure 26. This configuration is interesting because it was tested as a small, approximately 2-meter span, ejector powered model in reference 18 and as a large jet engine powered approximately 12-meter span model in the 40 by 80 wind tunnel in reference 17. Data from the later tests are available only for the tail on configuration with the flaps deflected. These data are compared with the small scale data and with tail on estimates in figure 27. Agreement between the small and large models is considerably better than with the tail on estimates which use the DATCOM estimate for the power off tail contribution. Estimates made using the small scale model power off, zero lift tail contribution are in much better agreement with both the small and large scale models.

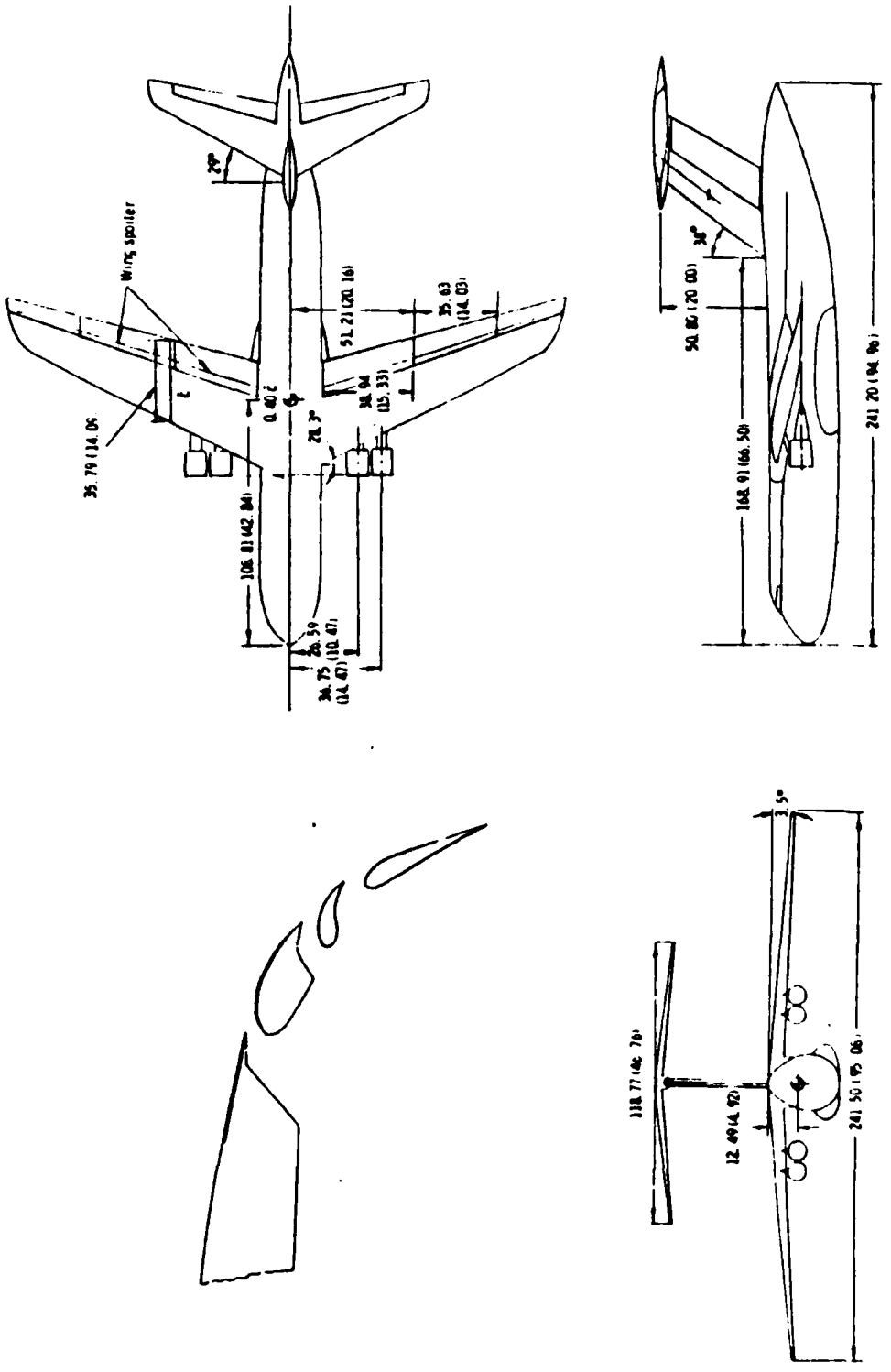

Figure 21 EBF Configuration of Ref. 10 and 11.
A = 7.23 $\Lambda_{c/2}$ = 22 Γ = -3.5

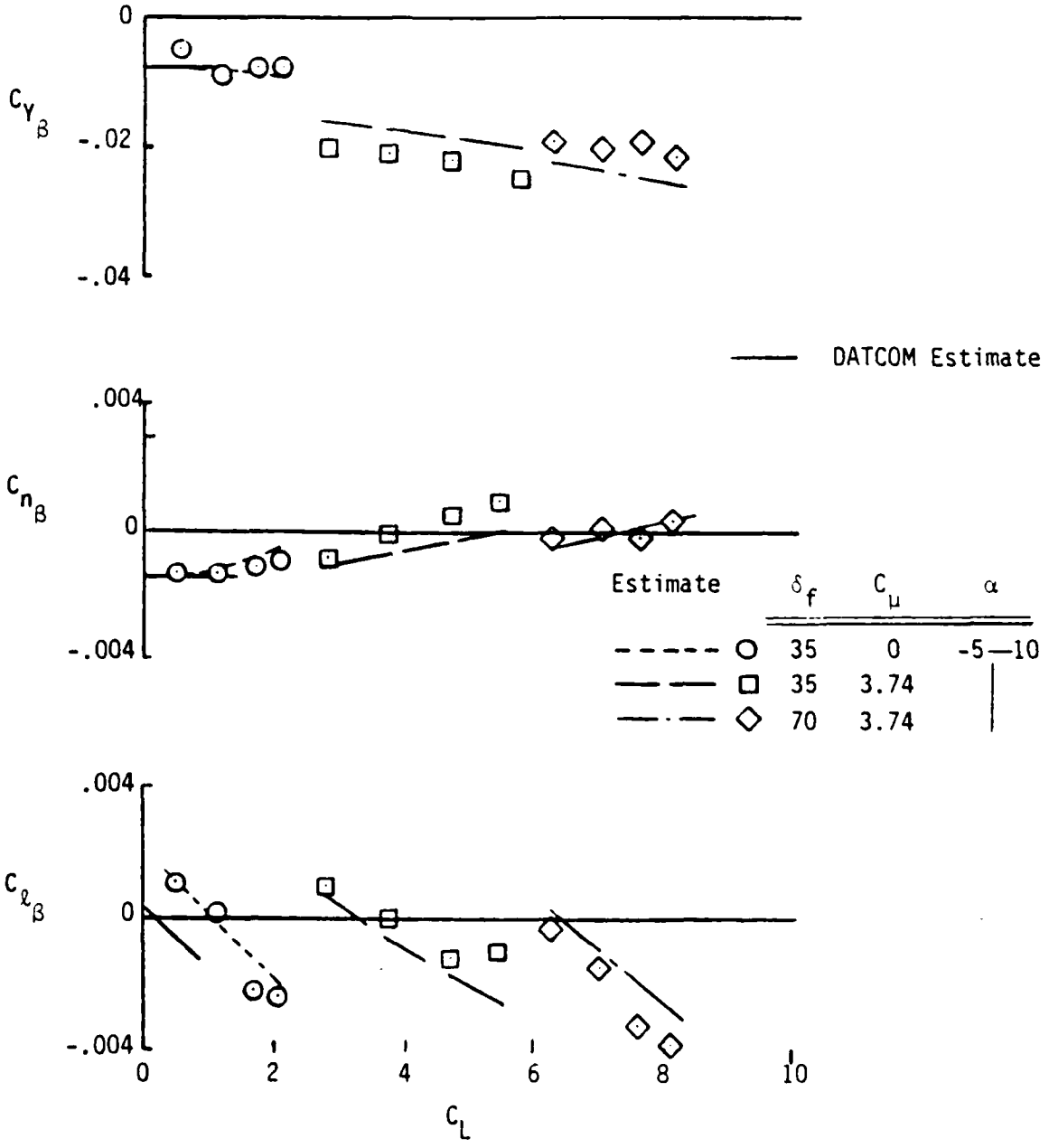

(a) Tail Off

Figure 22 Comparison of Estimates with Data for EBF Configuration Of Ref. 11.

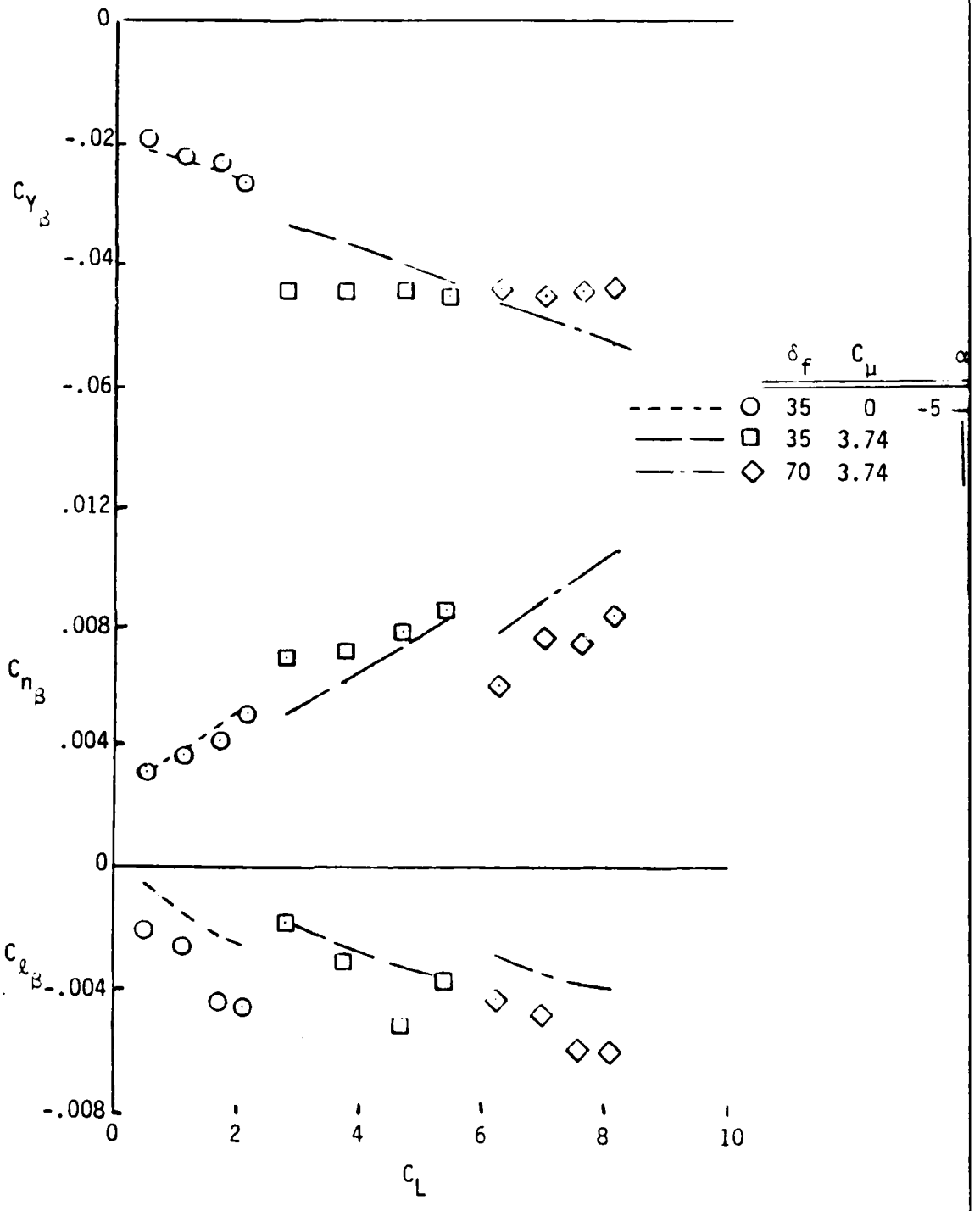

(b) Tail on

Figure 22 Concluded.

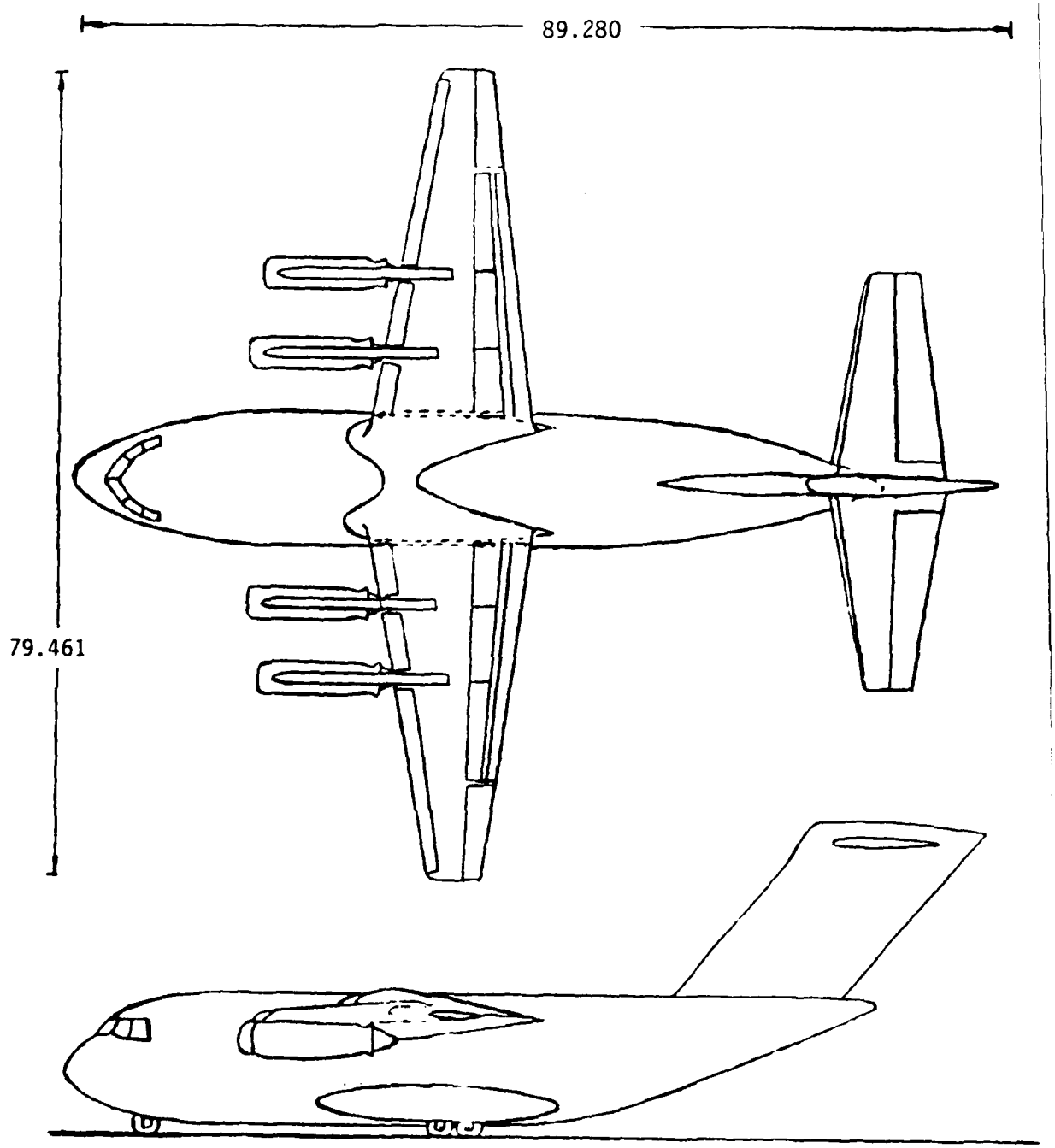

Figure 23 Configuration of the Model of Ref. 19. (YC-15)

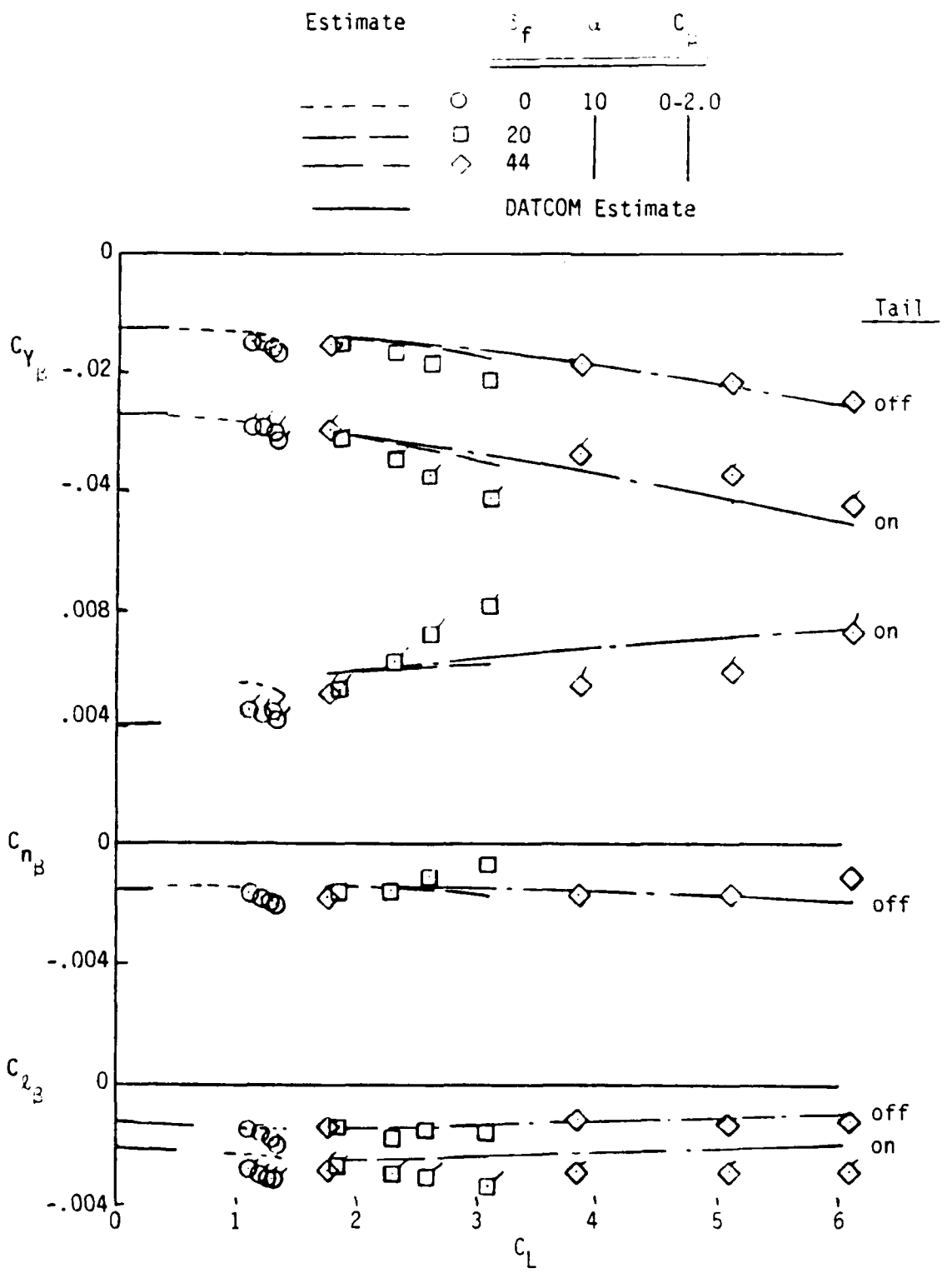

Figure 24 Comparison of Estimates with Data for EBF Configuration of Ref. 19. (YC-15)

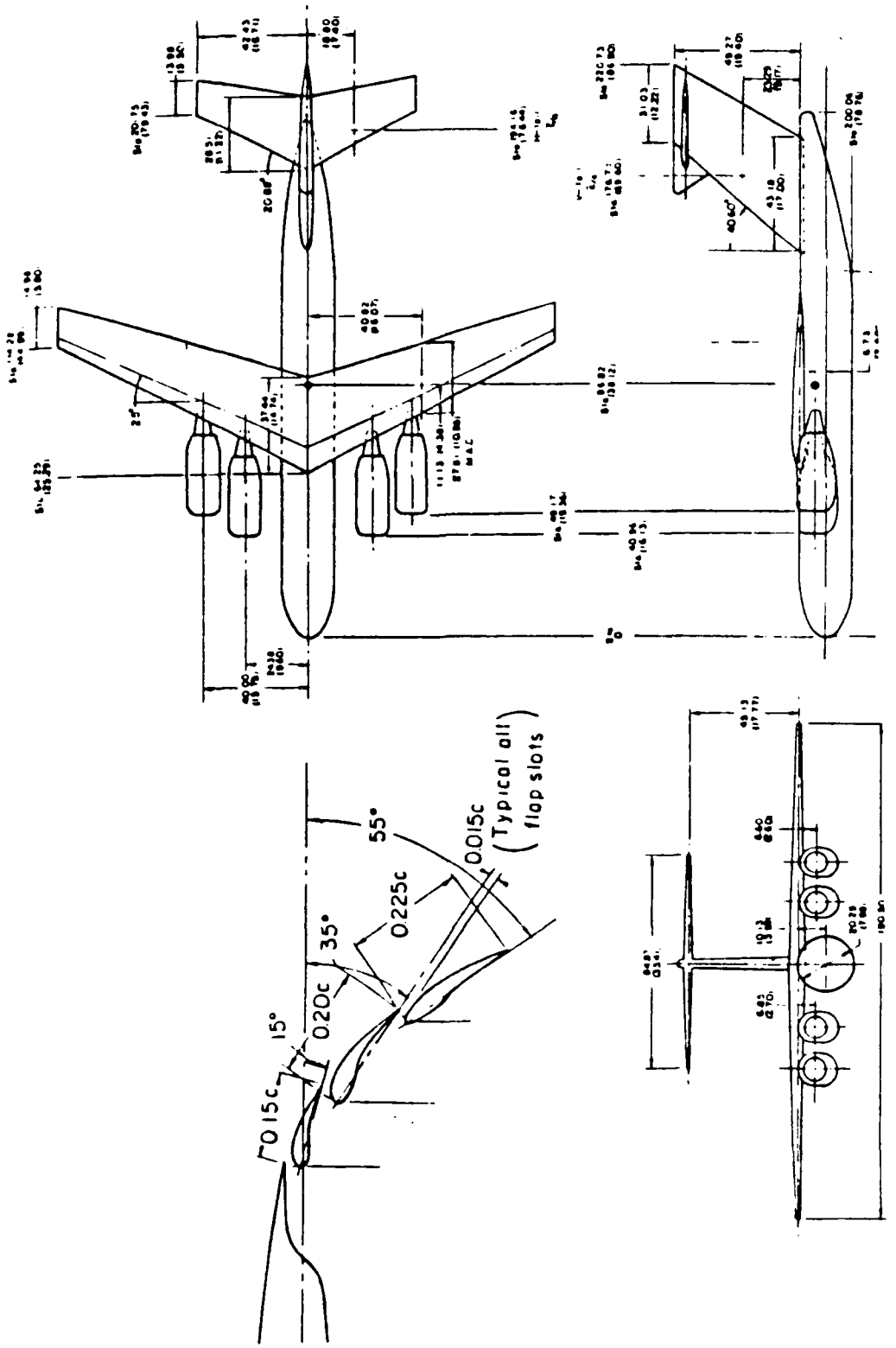

Figure 25 Configuration of EBF Models of Ref. 17 and 18.
$A = 7.0$ $\Lambda_{c/2} = 22$ $\Gamma = 0$

DATCOM	Present Estimate	δ_f	C_μ	α
———	- - - - - ○	0-55	0	0
	—— —— ◇	55	0-3.8	0
	—·—· Δ	55	3.8	0-15

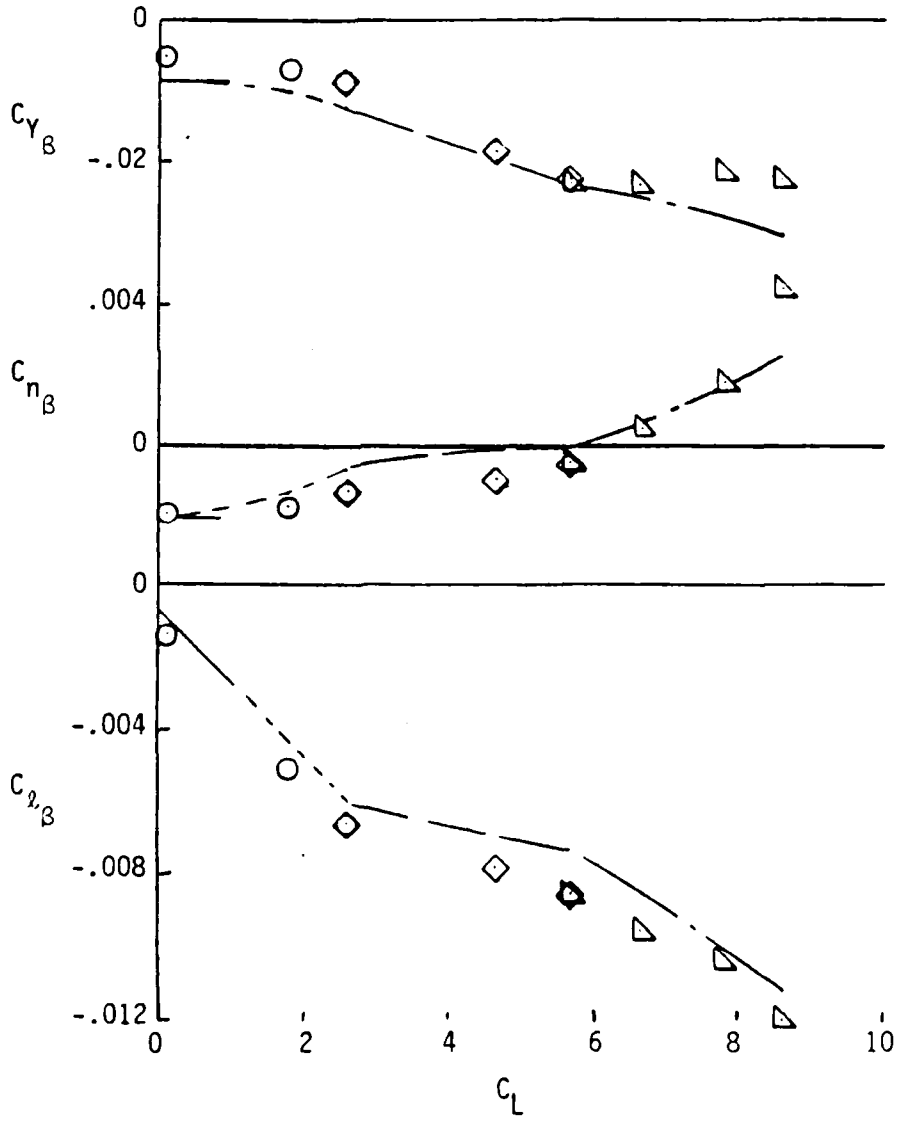

Figure 26 Comparison of Estimates with Data for EBF Model of Ref. 18. (Tail Off)

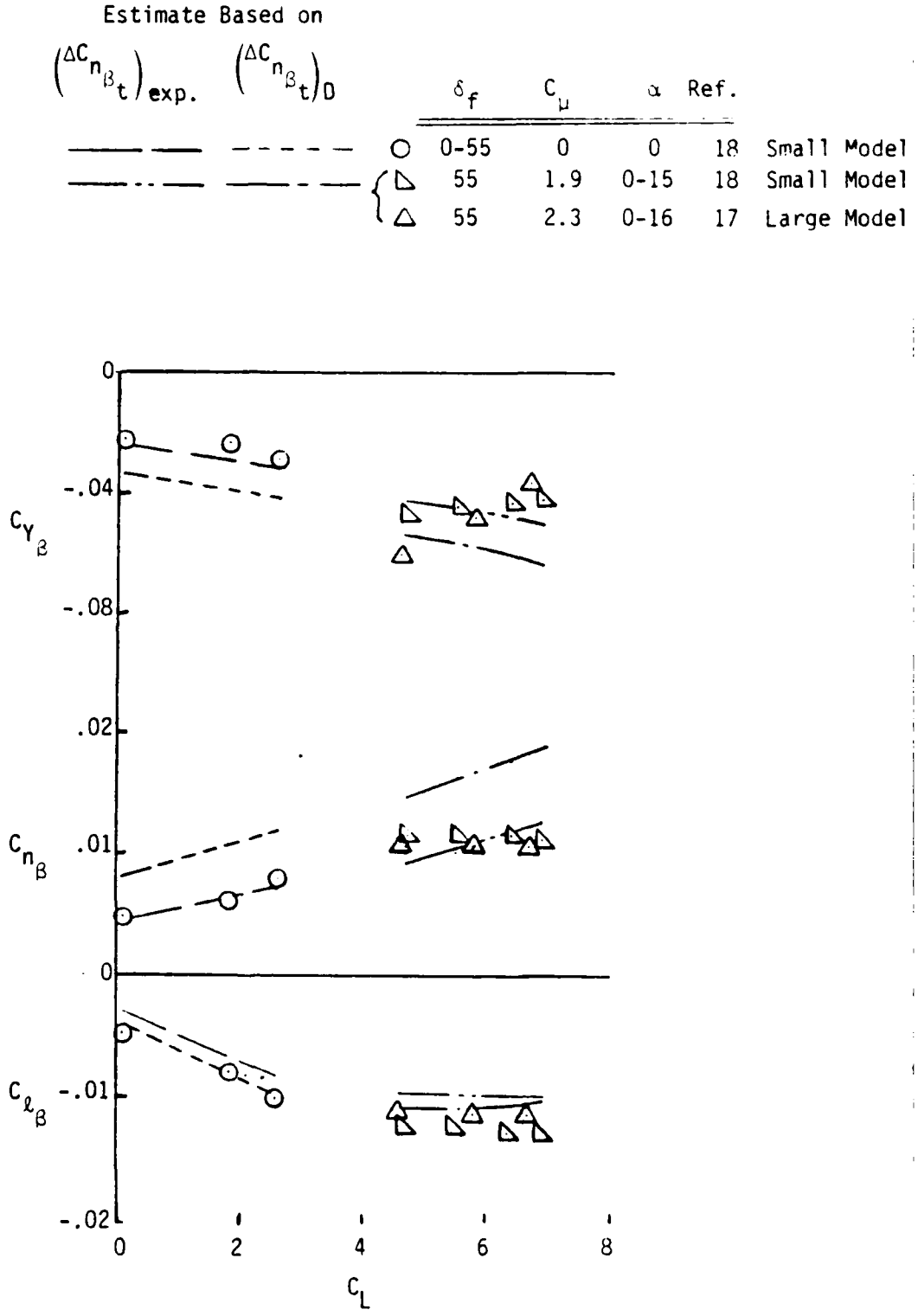

Figure 27 Comparison of Estimates with Data for EBF Model Ref. 17 & 18.

The configuration of references 17 and 18 has a relatively large vertical tail and a small fuselage; much smaller relative to the wing and tail than most of the other configurations used in developing the present method. The problem shown in figure 27 may illustrate a fundamental problem with the present method for estimating the tail contribution. The DATCOM method for estimating power off sidewash at the tail is presented in section 5.4.1 as:

$$\left(1 + \frac{\partial\sigma}{\partial\beta}\right)\frac{q_v}{q_\infty} = 0.724 + 3.06\,\frac{S_v/S_w}{1 + \cos\Lambda_{c/4}} + 0.4\,\frac{z_w}{d} + 0.009A$$

and for the configuration of references 17 and 18

$$\left(1 + \frac{\partial\sigma}{\partial\beta}\right)\frac{q_v}{q_\infty} = 0.724 + 0.708 - 0.2 + 0.065$$

$$= 1.297$$

The DATCOM method estimates a very large sidewash at the tail for this configuration for the power off case primarily because of the large ratio of vertical tail area to wing area (which appears in the second term). However, the sidewash arises from the "...side force developed by the body in yaw" as stated in the DATCOM text. But the body size, which determines the body side force does not appear in the expression for sidewash! Apparently, the correlation presented in DATCOM was developed from a data base that had much smaller ratio of tail to body size than that of references 17 and 18. Care should therefore be exercised in making estimates of the tail contribution and the experimental power off tail contribution for

the configuration for which estimates are being made should be used if it is available.

USB Configurations

The USB configuration shown in figure 28 (ref. 27) used the same fuselage, tail, and wing box as the large scale model of reference 17. New nacelles, nozzles, and flap system were installed to convert the model to an USB configuration. Comparison of estimates with the data for this configuration are shown in figure 29. As was the case with the EBF configuration (fig. 27), estimates based on the DATCOM estimate for the power off tail contribution considerably overestimate the directional stability. Flaps retracted, power off data were not measured on this configuration, but estimates made using the power off, flaps retracted data from reference 18 (which has the same body/tail configuration) are in much better agreement with the measured data. The differences between the estimates of the side force parameter and the data and the differences between the side force data for the two flap deflections cannot be explained.

The OSRA configuration and comparison of estimates with data are presented in figures 30 and 31. Although the wing is basically swept, the center section, where most of the powered lift is carried, is almost unswept. Estimates were made for both zero and 11.76-degree sweeps. The estimates for zero sweep are in better agreement with the measured effective dihedral, C_{L_β}, but significantly underestimate the directional stability. Unfortunately, tail off data are not available to determine whether this problem is in the estimate of the tail off data or in the estimate of the tail contribution.

The YC-14 configuration and comparisons of estimates with data are shown in figures 32 and 33. The directional stability and side force are seriously underestimated at the low momentum coefficient condition with the flaps down. Similar but less dramatic underestimates are present in some of the other comparisons (see for example figures 22b and 24) at moderate lift conditions. The problem appears to be in the estimate of the tail contribution. There appears to be an additional sidewash at moderate lift coefficients, perhaps from the nacelles or from the additional sideforce generated on these rather large fuselages. Attempts to develop an adjustment to the method to account for this additional sidewash were unsuccessful because of the meager data base.

IBF Configurations

The configuration of the British H-126 jet flap research airplane is shown in figure 34. Data from wind tunnel tests (ref. 29) of models preceding the development of this airplane provided much of the IBF data used in developing the method. The comparison of estimates with data for one of the configurations of reference 29 is presented in figure 35 and gives an indication of the best that can be expected of the method.

The complete airplane was tested in the Ames Research Center 40 by 80 tunnel after the completion of the flight test program. Tail off data were not obtained. The estimates compared with the measured data in figure 36 are based on the DATCOM estimate of the tail contribution.

CCW Configuration

Lateral/directional data are available for only one Circulation Control Wing (CCW) configuration: the A-6 CCW demonstrator airplane of

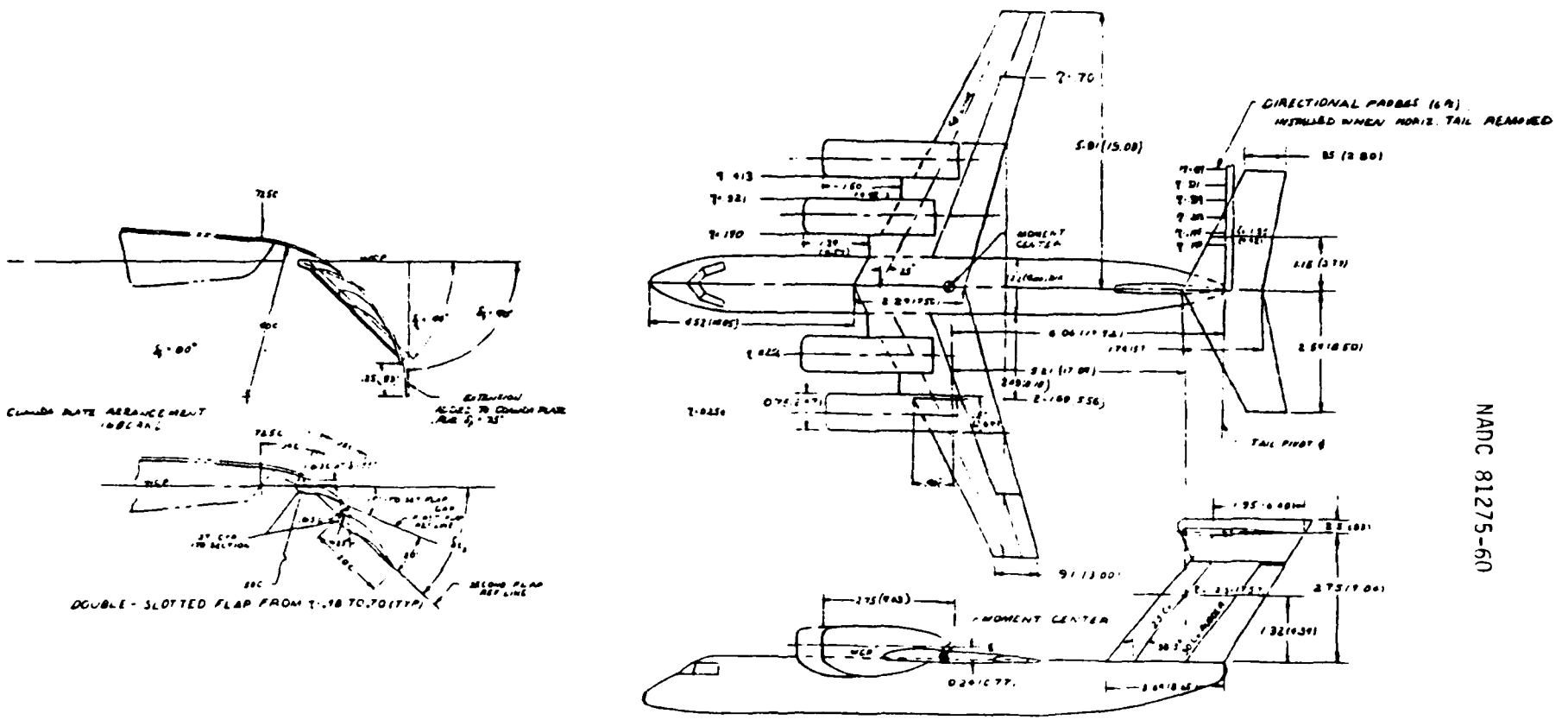

Figure 28 Configuration of Large Scale USB Model of Ref. 27.

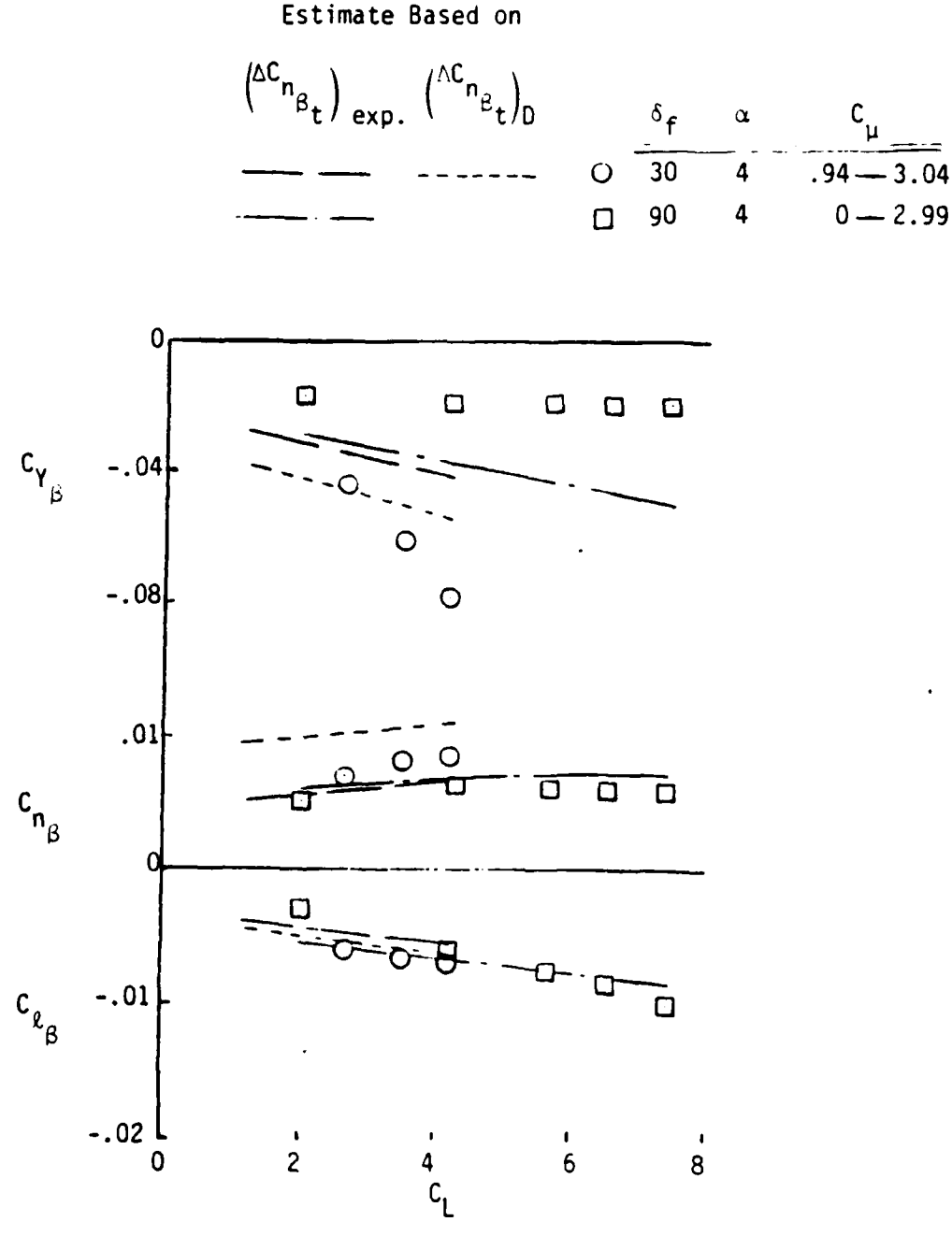

Figure 29 Comparison of Estimates with Data from the USB Model of Ref.

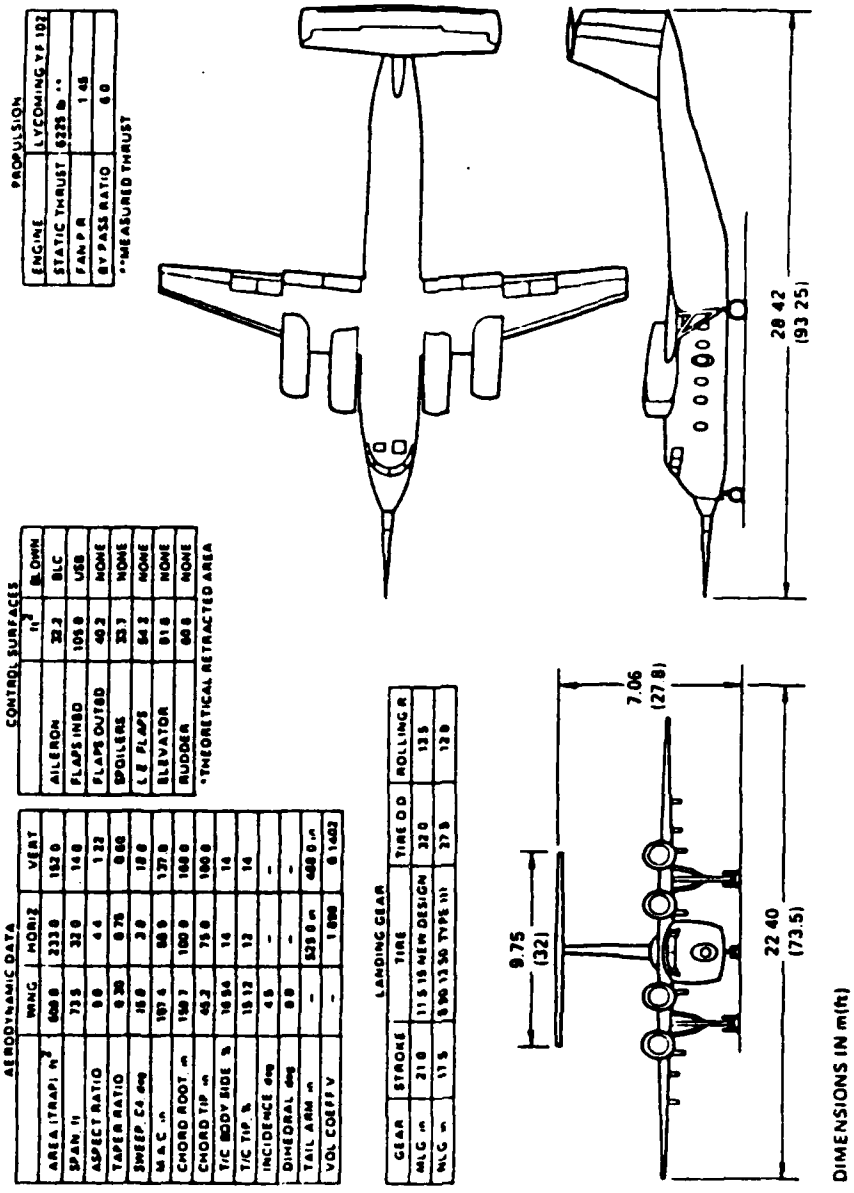

Figure 30 Configuration of the Airplane of Ref. 21 (QSRA).

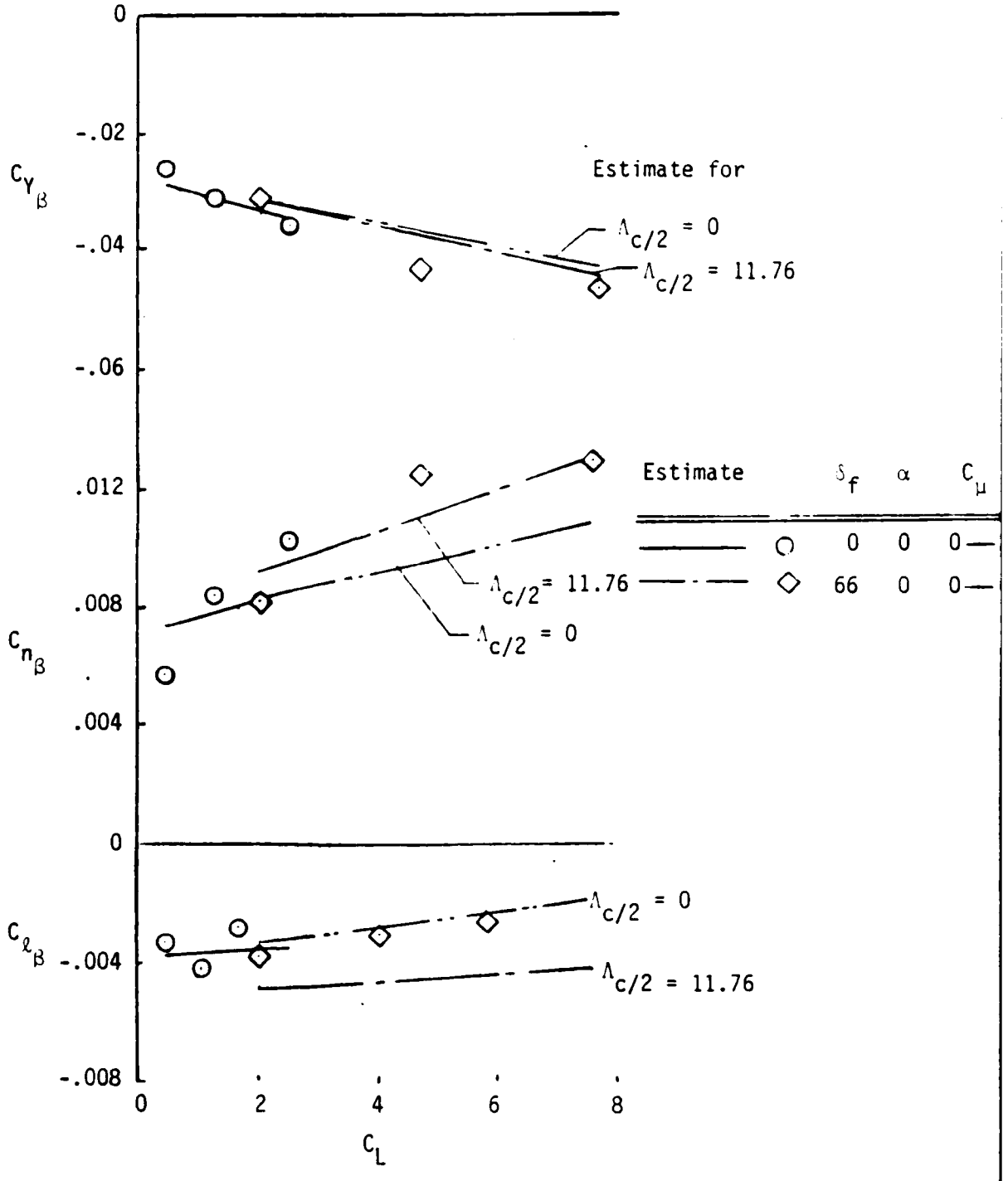

Figure 31 Comparison of Estimates with Data for the USB Configuration of Ref. 21. (QSRA)

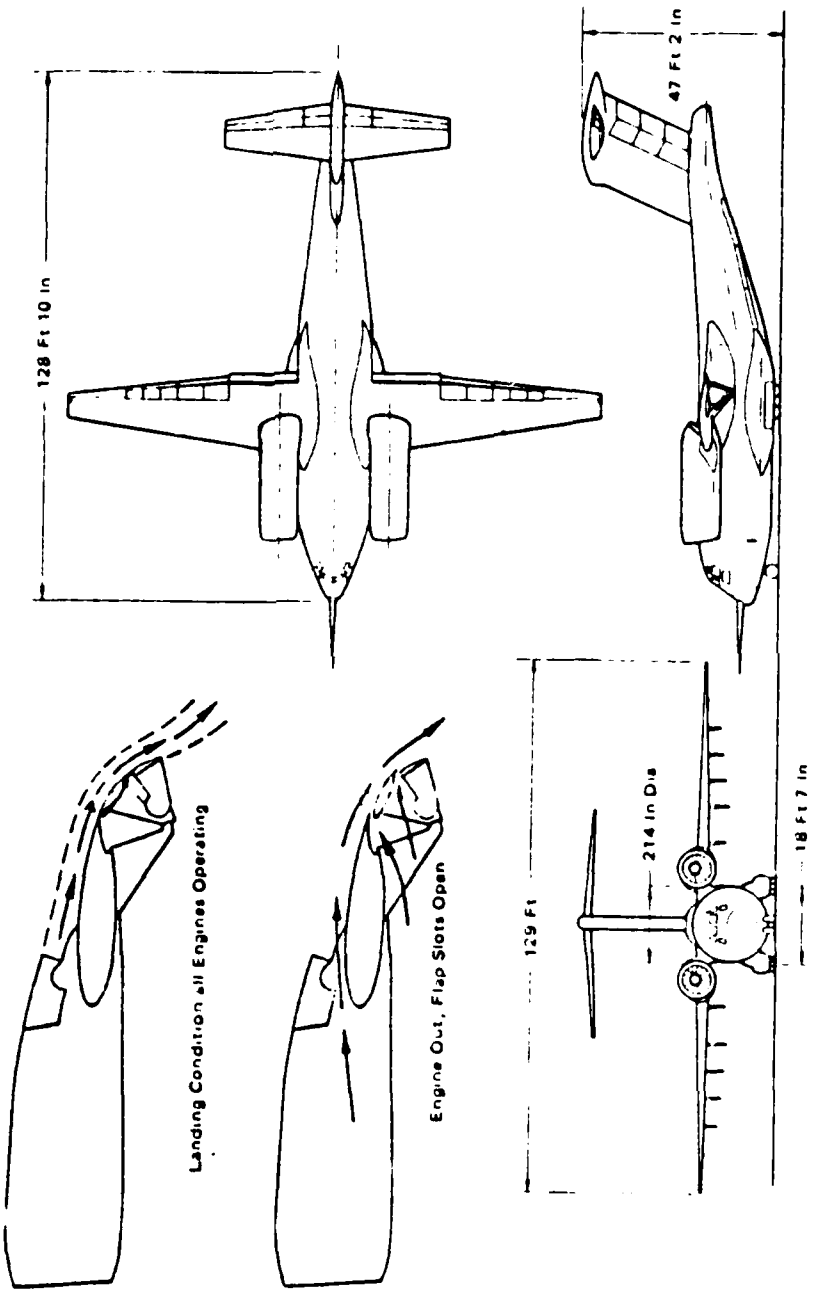

Figure 32 Boeing AMST Prototype - YC-14.

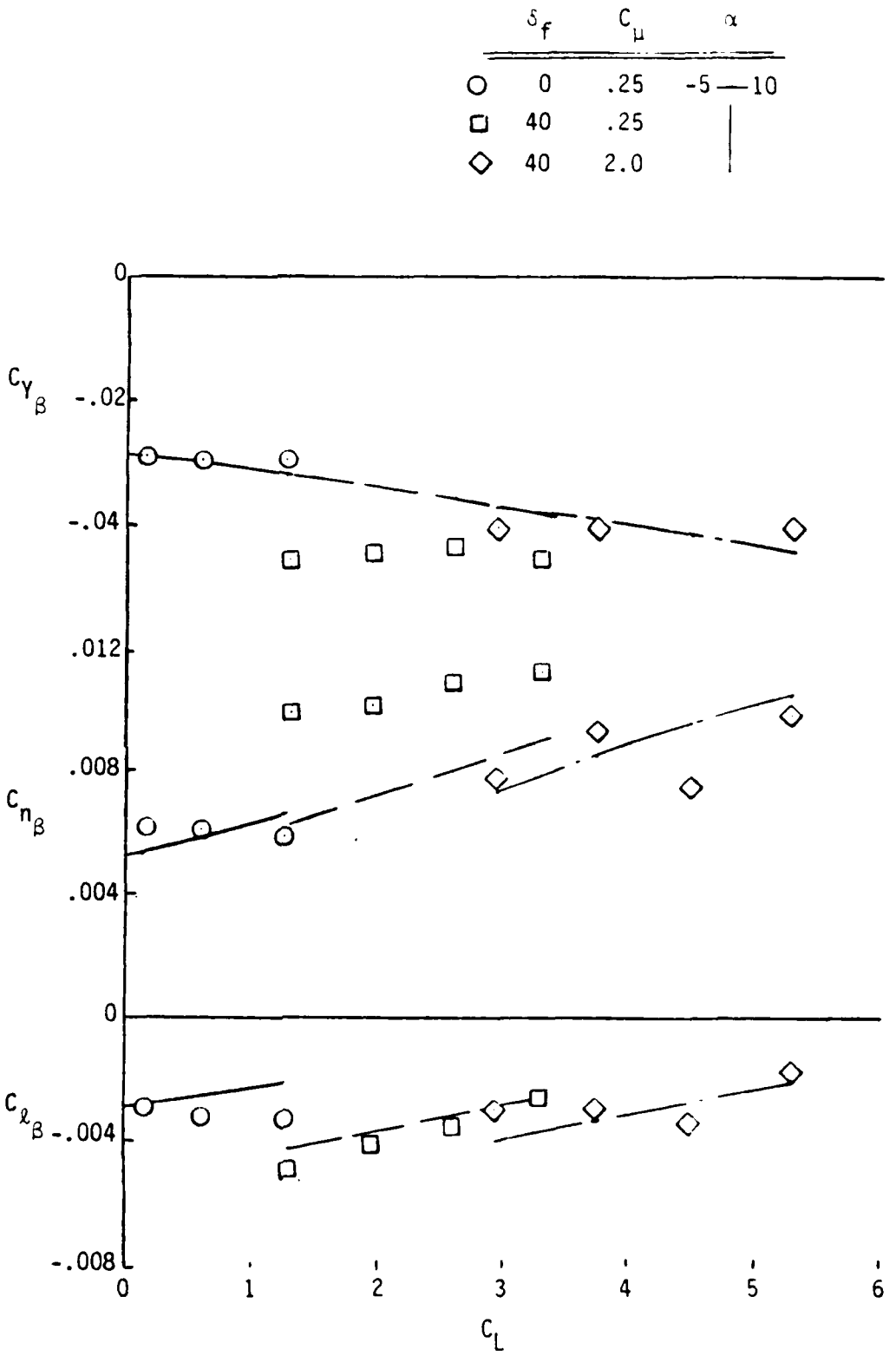

Figure 33 Comparison of Estimates with Data for USB Model of Ref. 20. (YC-14)

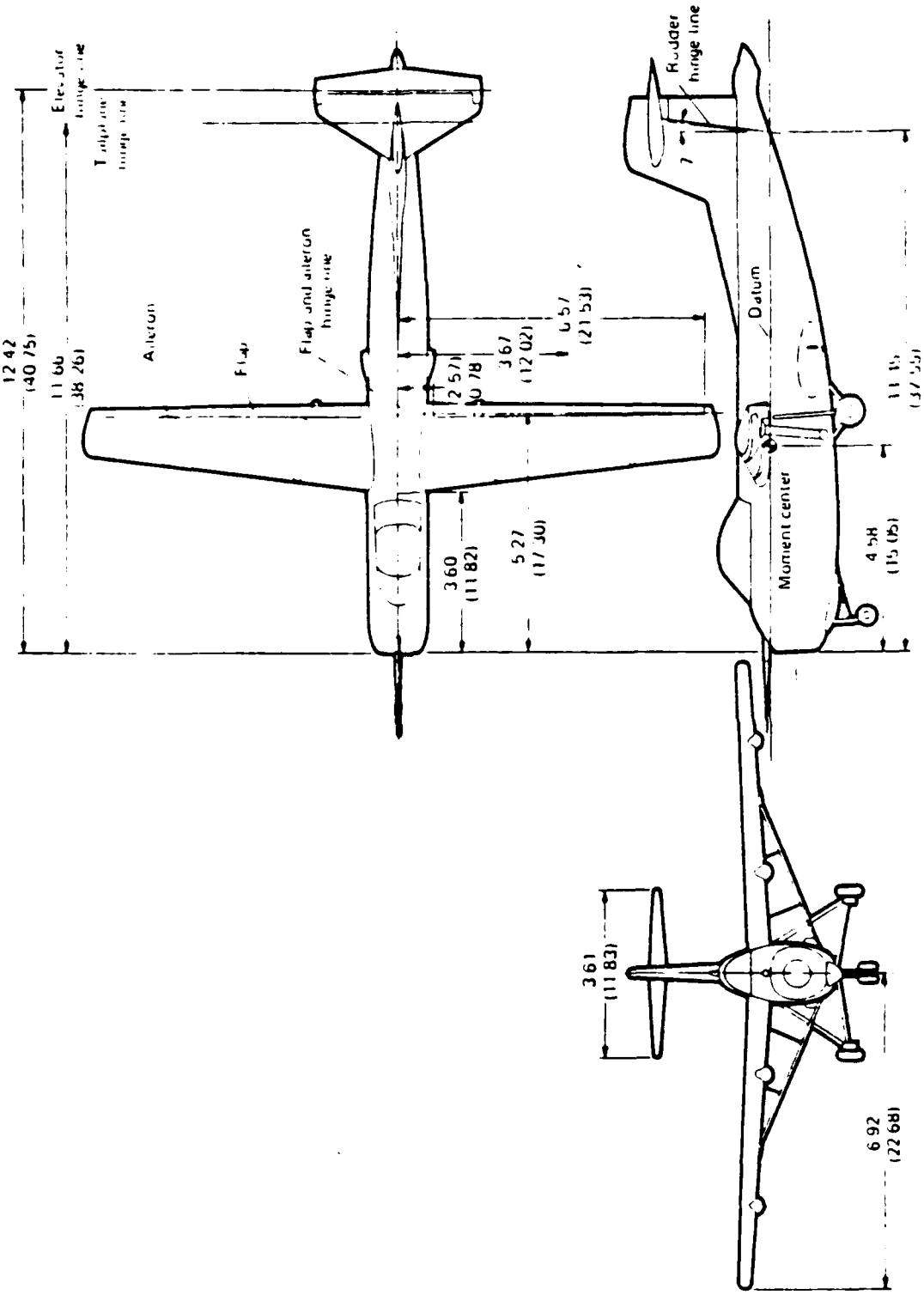

Figure 34 Configuration of the Airplane of Ref. 30.

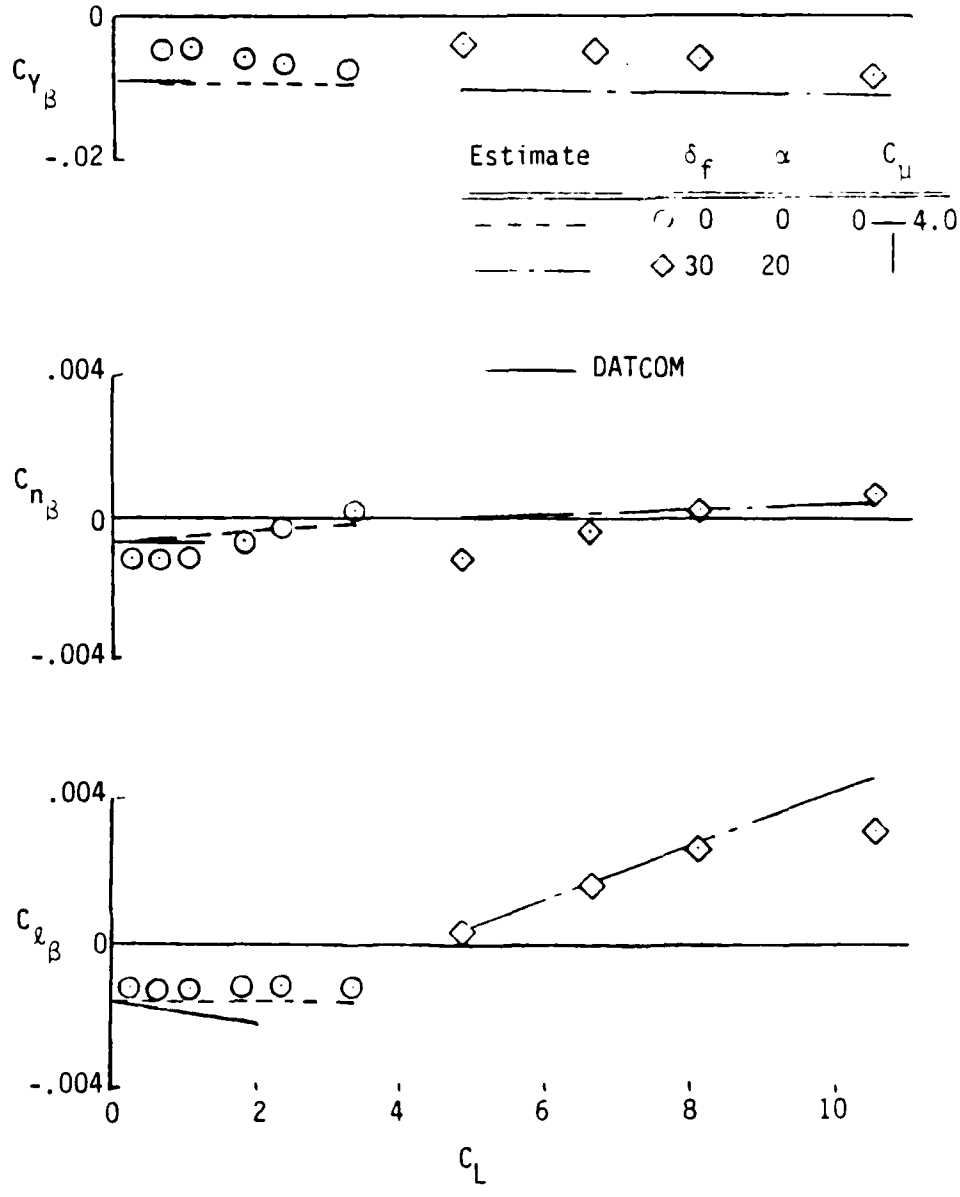

Figure 35 Comparison of Estimates with Data for the IBF Configuration of Ref. 29 ;

$\Lambda_{c/2}$ = 3.5 A = 9.2 Γ = +4 (Tail Off)

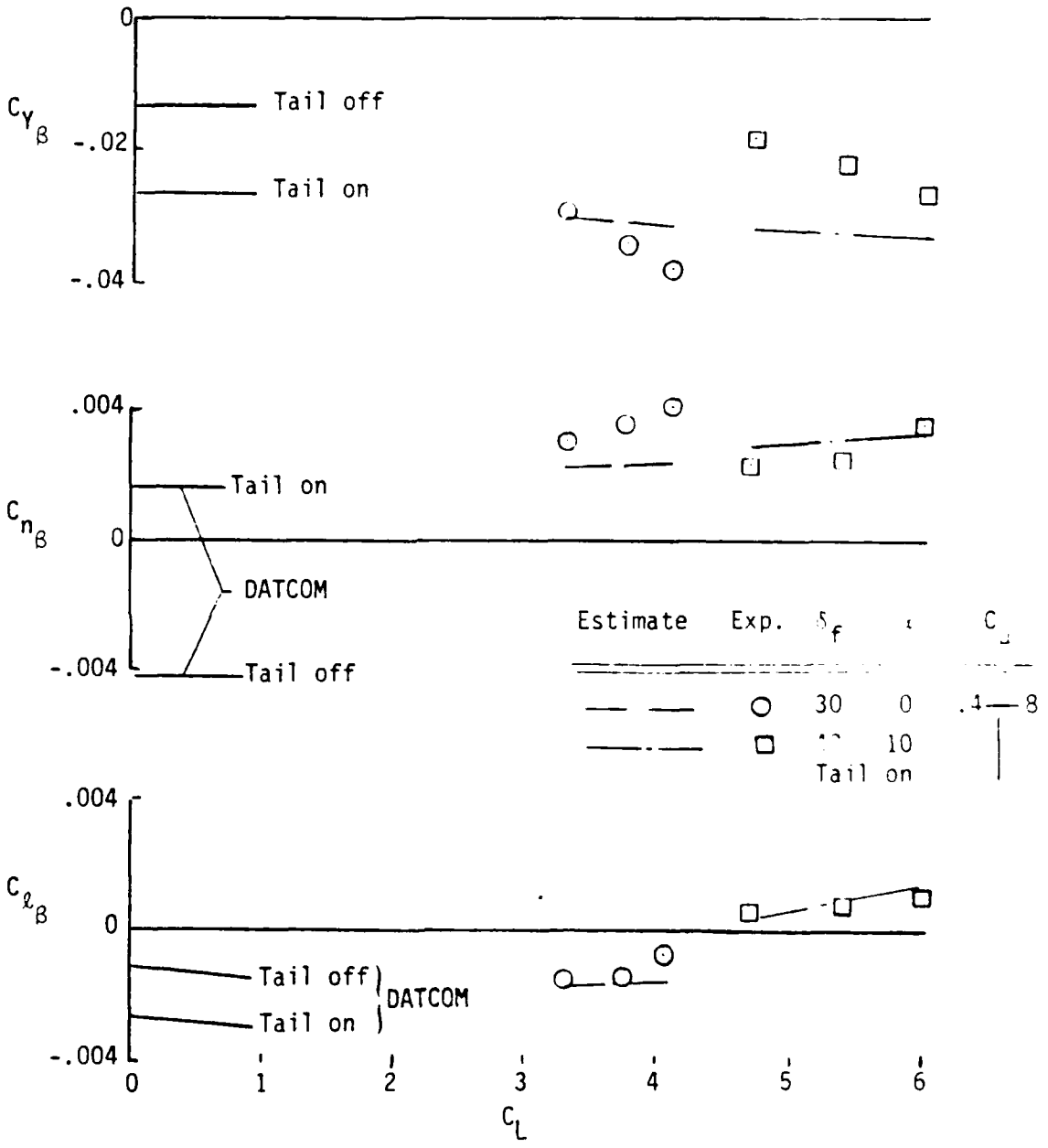

Figure 36 Comparison of Estimates with Data for the IBF Configuration of Ref. 30.

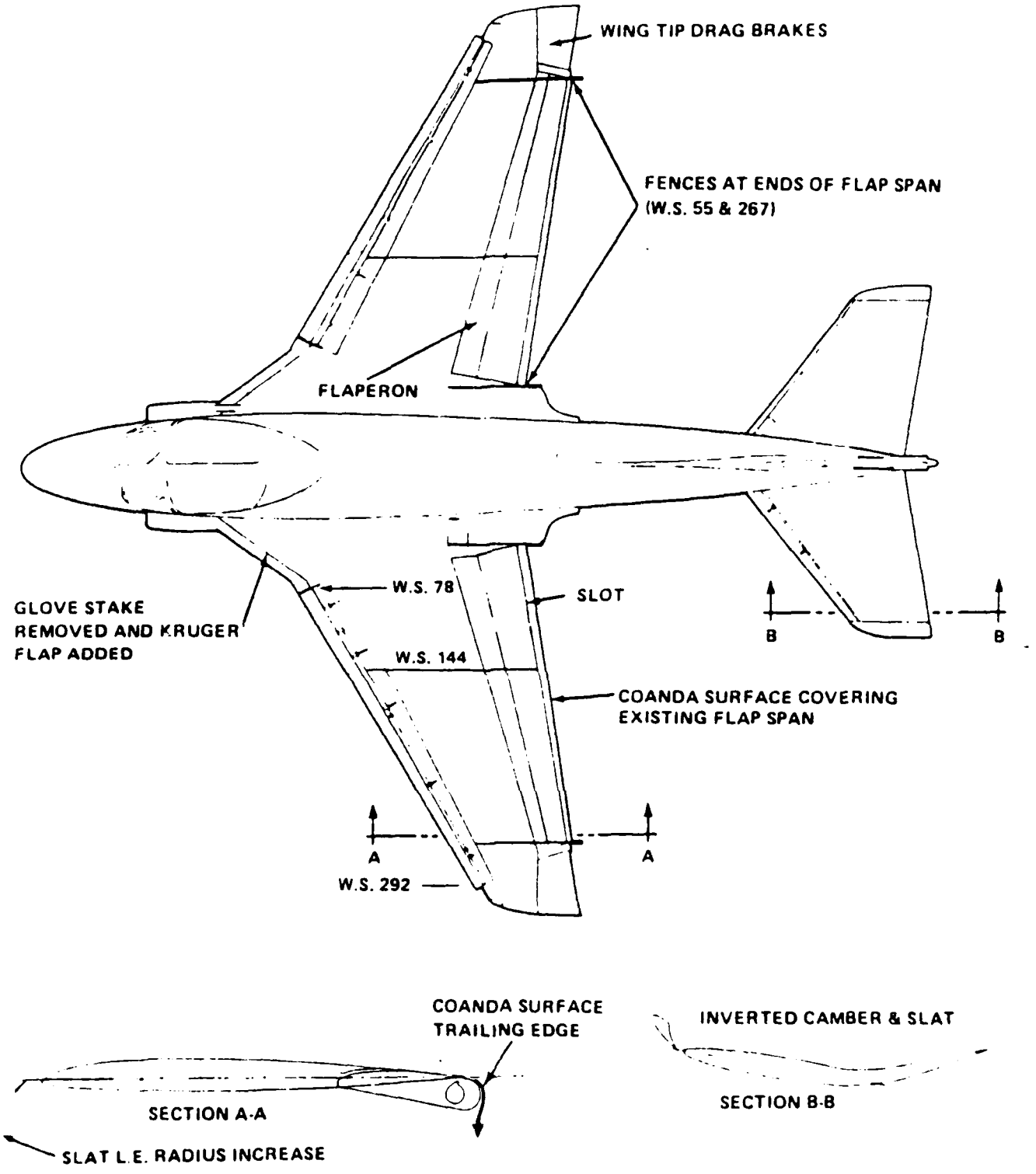

Figure 37 Configuration of the Model of Ref. 31. (CCW)

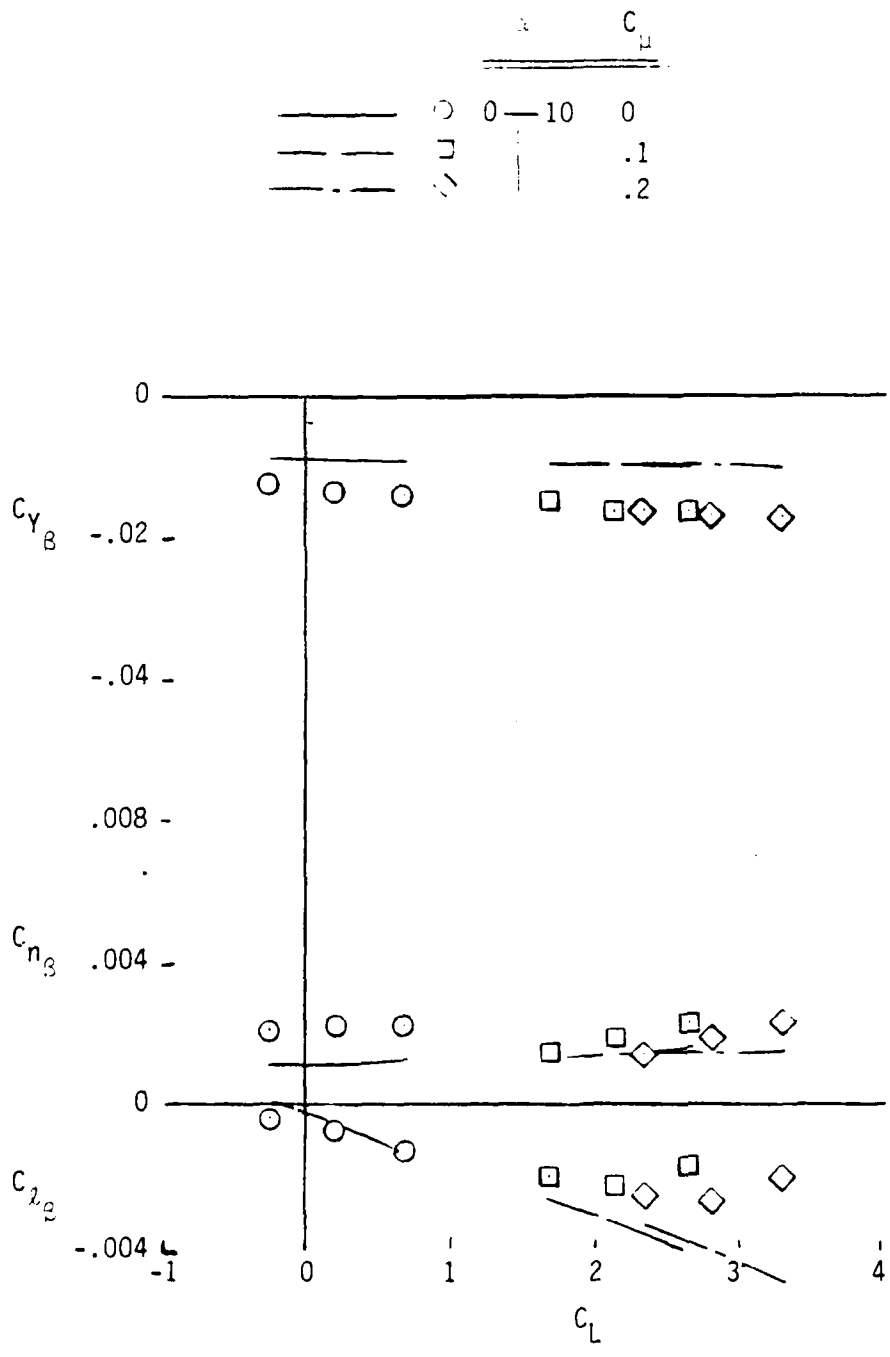

Figure 38 Comparison of Estimates with Data for CCW Configuration of Ref. 31. (Tail on)

reference 31 shown in figure 37. This concept does not use conventional flaps, but has a blowing slot at the wing trailing edge which blows over a cylindrical trailing edge. The jet sheet deflection depends on the free stream dynamic pressure (at zero speed, the jet sheet will turn through 180 degrees) and significant lifts can be generated with very low blowing momentum coefficients. The comparison of the estimated lateral/directional characteristics with the data from reference 31 is presented in figure 38. Unfortunately, there is not tail off data available but the underestimate of the side force and directional stability at zero lift is believed to be due to an underestimate of the tail contribution by the DATCOM method. Because the increment of side force factor due to power on $\Delta C_{Y_{\beta_\mu}}$ and the corresponding increment of the directional stability parameter, $\Delta C_{n_{\beta_\mu}}$ is believed to be carried primarily on the flap system and, as there is no physical flap on this configuration, these terms were set at zero in the power on estimates. If they had been taken at face value, the directional stability would have been significantly overestimated at the higher lift coefficients. Because the deflection of the jet sheet was unknown, the estimate of the increment of effective dihedral parameter, $\Delta C_{\ell_{\beta_\mu}}$ assumed the jet sheet deflection was zero. The results show that the effective dihedral is overestimated, indicating that there is an effect of jet sheet deflection but there is no way to determine what it is.

PRESENTATION OF THE METHOD

The method is recapped here for the convenience of the user.

Side Force

The tail off value of the side force parameter C_{Y_β} is given by

$$C_{Y_\beta} = C_{Y_{\beta_D}} + \Delta C_{Y_{\beta_o}} + \Delta C_{Y_{\beta_i}} + \Delta C_{Y_{\beta_\mu}}$$

where

$C_{Y_{\beta_D}}$ is the DATCOM estimate from section 5.2.1.1 including the contribution of the engine nacelles.

$$\Delta C_{Y_{\beta_o}} = -0.00044(C_{L_o})^2$$

$$\Delta C_{Y_{\beta_i}} = -\frac{\dot{m}V}{qs}\ \frac{1}{57.3}$$

and

$\Delta C_{Y_{\beta_\mu}} = -0.002\Delta C_{L_\mu}$ for EBF configurations

$\Delta C_{Y_{\beta_\mu}} = -\ 0.038(1 - \cos \Lambda_{c/2})\ \Delta C_{\ell_\mu}$ for IBF configurations

$\Delta C_{Y_{\beta_\mu}} = -\ .019(1 - \cos \Lambda_{c/2})\ \Delta C_{L_\mu}$ for USB configurations.

Directional Stability

The tail off value of the directional stability parameter is given by:

$$C_{n_\beta} = C_{n_{\beta_D}} + \Delta C_{n_{\beta_o}} + \Delta C_{n_{\beta_i}} + \Delta C_{n_{\beta_\mu}}$$

where

$C_{n_{\beta_D}}$ is the DATCOM estimate from section 5.2.3.1 including the contribution of the engine nacelles.

$$\Delta C_{n_{\beta_o}} = 0.00001 \Lambda_{c/2} (C_{L_o})^2$$

$$\Delta C_{n_{\beta_i}} = \Delta C_{Y_{\beta_i}} \left(\frac{x_i}{b} \cos \alpha - \frac{z_i}{b} \sin \alpha \right)$$

and

$$\Delta C_{n_{\beta_\mu}} = 0.000074 \Lambda_{c/2} \sqrt{\frac{b_j}{b}} \sqrt{\Delta C_{\ell_\mu}} \quad \text{for EBF and IBF configurations}$$

$$\Delta C_{n_{\beta_\mu}} = 0.000028 \Lambda_{c/2} \sqrt{\frac{b_j}{b}} \sqrt{\Delta C_{\ell_\mu}} \quad \text{for USB configurations}$$

Effective Dihedral

And the tail off value of the effective dihedral parameter is given by:

$$C_{\ell_\beta} = C_{\ell_{\beta_o}} + \left(\frac{C_{\ell_\beta}}{C_L} \right)_D C_{L_o} + \Delta C_{\ell_{\beta_f}} + \Delta C_{\ell_{\beta_i}} + \Delta C_{\ell_{\beta_\mu}}$$

where

$C_{\ell_{\beta_o}}$ is the DATCOM estimate of C_{ℓ_β} at zero lift from section 5.2.2.1

$\left(\frac{C_{\ell_\beta}}{C_L} \right)_D$ is the DATCOM estimate of the effect of lift coefficient on C_{ℓ_β} from section 5.2.2.1.

$$\Delta C_{\ell_{\beta_f}} = 0.32 \left(\frac{C_{\ell_\beta}}{C_L} \right)_D |\Gamma| (\cos \Lambda_{c/2})^2 \Delta C_{L_f}$$

$$\Delta C_{\ell_{\beta_i}} = \Delta C_{Y_{\beta_i}} \left(\frac{z_i}{b} \cos \alpha + \frac{x_i}{b} \sin \alpha \right)$$

and

$$\Delta C_{\ell_{\beta_\mu}} = [K_{\ell_\Lambda} + 0.000092A - 0.000035\Gamma + K_\theta(\frac{\theta + \alpha}{100})^2]\Delta C_{L_\mu}$$

where

K_{ℓ_Λ} = -0.00065 - 0.0195(1 - cos $\Lambda_{c/2}$) for IBF configurations

K_{ℓ_Λ} = -0.00045 - 0.009(1 - cos $\Lambda_{c/2}$) for EBF and USB configurations

and

K_θ = 0.0015 for IBF configurations

K_θ = 0 for EBF and USB configurations

Tail Contribution

The tail contribution increases because of a strong sidewash induced at high lift conditions. The tail contributions are based on the DATCOM estimate of the power off tail contribution and are given by:

$$\Delta C_{Y_{\beta_t}} = \left(\Delta C_{Y_{\beta_t}}\right)_D (1 + K_\sigma)$$

$$\Delta C_{n_{\beta_t}} = \left(\Delta C_{Y_{\beta_t}}\right)_D (1 + K_\sigma)\ (\frac{x_t}{b} \cos \alpha + \frac{z_t}{b} \sin \alpha)$$

$$\Delta C_{\ell_{\beta_t}} = \left(\Delta C_{Y_{\beta_t}}\right)_D (1 + K_\sigma)\ (\frac{z_t}{b} \cos \alpha - \frac{z_t}{b} \sin \alpha)$$

where

$\left(\Delta C_{Y_{\beta_t}}\right)_D$ is the DATCOM estimate of the tail contribution from section 5.3.1.1

and

K_σ is the lift induced sidewash factor and is given by:

$$K_\sigma = \frac{0.0135}{\frac{b_j}{b} \quad \frac{x_j}{b}} C_L$$

DISCUSSION OF LIMITATIONS

The present study has examined the lateral/directional data on a wide variety of powered lift STOL configurations in an attempt to identify the primary factors that determine the lateral/directional characteristics at high power, high lift conditions. A number of anomalies have been encountered in developing the correlations presented here. Because these anomalies could not be explained, it was necessary in some cases to ignore what appears to be perfectly good data in arriving at the expressions that make up the present method. Data obtained in the future may explain these anomalies or show that data ignored should have been used and data used was not valid. The user should keep in mind the problems discussed in the preceding sections and be prepared to make adjustments as more pertinent data becomes available to him.

Like the DATCOM method which provides the power off starting point for the present method, it is limited to the low to moderate angle of attack range where the flow on the wing-flap system is unseparated. The data base consisted primarily of high wing transport type configurations. The effects of moving the wing to a low position are unknown and application of the method o wings with aspect ratios below about 7 and sweep angles above about 30 degrees should be made with caution.

The present method is intended for use only in preliminary design work and to give a general indicatio. of the effects of the primary configuration variables. The aerodynamic characteristics of STOL configurations are a complex function of many configuration variables and the development of any distributed jet STOL aircraft will require careful experimental investigations to accurately determine the lateral/directional forces and moments.

CONCLUDING REMARKS

This study has examined the possibility of developing a method for estimating the lateral/directional stability characteristics of distributed jet (jet flap) STOL configurations and developed a method that is believed to account for the major effects of operating at high power-on lift coefficients. In addition to inducing a large stabilizing side wash at the vertical tail, powered lift reduces the directional instability contribution of the wing/body, increases the side force due to sideslip and tends to reduce (depending on the amount of geometric dihedral incorporated) the high level of effective dihedral normally associated with swept wings at high lift coefficients.

The method is intended for use only in preliminary design and not as a substitute for a carefully conducted wind tunnel program which will still be required in the development of any powered lift aircraft. The data base on which the method is based is primarily from model tests of high wing transport configurations. The effects of moving the wing to a low position are unknown and application of the method to configurations with wings having aspect ratios less than about 7 and sweep angles above about 30 degrees should be made with caution.

REFERENCES

1. Henderson, C., Clark, J. and Walters, M., "V/STOL Aerodynamics and Stability and Control Manual," NADC Rpt. No. NADC-80017-60, Jan. 1980.

2. "USAF Stability and Control DATCOM," Oct. 1960, revised Jan. 1975.

3. Hebert, J., Jr. et al., "STOL Tactical Aircraft Investigation, Volume II - Design Compendium," Convair Division of General Dynamics. AFFDL TR 73-21 Vol. II, May 1973.

4. Roe, H. M., et al., "STOL Tactical Aircraft Investigation, Volume II - Design Compendium," Los Angeles Aircraft Division, Rockwell International, AFFDL TR 73-20, Vol. II, April 1973.

5. Polhamus, E. C. and Sleeman, W. C., Jr., "The Rolling Moment Due to Sideslip of Swept Wings at Subsonic and Transonic Speeds," NASA TN-D-209, Feb. 1960.

6. Toll, T. A. and Queijo, M. J., "Approximate Relations and Charts for Low-Speed Stability Derivatives of Swept Wings," NACA TN 1581, May 1948.

7. Lichtenstein, J. H. and Williams, J. L., "Effect of High-Lift Devices on the Static-Lateral-Stability Derivatives of a 45° Sweptback Wing of Aspect Ratio 4.0 and Taper Ratio 0.6 in Combination With a Body," NACA TN 2819, Nov. 1952.

8. Freeman, D. C., Grafton, S. B., and D'Amato, R., "Static and Dynamic Stability Derivatives of a Model of a Jet Transport Equipped with External-Flow Jet-Augmented Flaps," NASA TN D-5408, Sept. 1969.

9. Parlett, L. P., Freeman, D. C., Jr., and Smith C. C., Jr., "Wind-Tunnel Investigation of a Jet Transport Airplane Configuration with High Thrust-Weight Ratio and an External-Flow Jet Flap," NASA TN D-6058, Nov. 1970.

10. Parlett, L. P. et al., "Wind-Tunnel Investigation of an External-Flow Jet-Flap Transport Configuration Having Full-Span Triple-Slotted Flaps," NASA TN D-6391, Aug. 1971.

11. Grafton, S. B., Parlett, L. P., and Smith C. C., Jr., "Dynamic Stability Derivatives of a Jet Transport Configuration with High Thrust-Weight Ratio and an Externally Blown Jet Flap," NASA TN D-6440, Sept. 1971.

12. Parlett, L. P., Emerling, S. J., and Phelps, A. E. III, "Free-Flight Investigation of the Stability and Control Characteristics of a STOL Model with an Externally Blown Jet Flap," NASA TN D-7411, April 1974.

13. Parlett, L. P., and Shivers, J. P., "Wind-Tunnel Investigation of an STOL Aircraft Configuration Equipped with an External-Flow Jet Flap," NASA TN D-5364, Aug. 1969.

14. Johnson, J. L., Jr., "Wind-Tunnel Investigation at Low Speeds of Flight Characteristics of a Sweptback-Wing Jet-Transport Airplane Model Equipped with an External-Flow Jet-Augmented Slotted Flap," NACA TN 4255, July 1958.

15. Hebert, J., Jr. et al., "STOL Tactical Aircraft Investigation, Volume IV - Wind Tunnel Data Analysis," Convair Division of General Dynamics. AFFDL TR-73-21-Vol. IV, May 1973.

16. Eilert, M. B., "Low Speed Wind Tunnel Tests of a Powered 1/20 Scale STOL Tactical Transport Model...," General Dynamics Corporation, GDLST 612, 612-1, 612-3, 612-4, 612-5, 612-6, Jan. 1973.

17. Aoyagi, K., Falarski, M. D., and Koenig, D. G., "Wind-Tunnel Investigation of a Large-Scale 25° Swept-Wind Jet Transport Model with an External Blowing Triple-Slotted Flap," NASA TM X-62,197, Nov. 1973.

18. Gentry, G. L., Jr., "Wind-Tunnel Investigation of an Externally Blown Flap STOL Transport Model Including an Investigation of Wall Effects," NASA TM X-3009, Sept. 1974.

19. Unpublished Data From Tests of Model of the YC-15 Configuration, Courtesy of Douglas Aircraft Company.

20. Unpublished Data From Tests of Model of the YC-14 Configuration, Courtesy of The Boeing Military Airplane Company.

21. Unpublished Data From Tests of Model of the QSRA Configuration, Courtesy of The Boeing Military Airplane Company.

22. Unpublished Data From Tests of Model of a Four Engine USB Configuration, Courtesy of The Boeing Military Airplane Company.

23. Phelps, A. E. III and Smith, C. C., Jr., "Wind-Tunnel Investigation of an Upper Surface Blown Jet Flap Powered-Lift Configuration," NASA TN D-7399, Dec. 1973.

24. Sleeman, W. C., Jr. and Holweg, W. C., "Low-Speed Wind-Tunnel Investigation of a Four Engine Upper Surface Blown Model Having a Swept Wing and Rectangular and D-Shaped Exhaust Nozzles," NASA TN D-8061, Dec. 1975.

25. Parlett, L. P., "Free-Flight Wind-Tunnel Investigation of a Four-Engine Sweptwing Upper Surface Blown Transport Configuration," NASA TN D-8479, Aug. 1977.

26. Aoyagi, K., Falarski, M. D. and Koenig, D. G., "Wind Tunnel Investigation of a Large-Scale Upper Surface Blown-Flap Transport Model Having Two Engines," NASA TM X-62,296, Aug. 1973.

27. Aoyagi, K., Falarski, M. D. and Koenig, D. G., "Wind Tunnel Investigation of a Large-Scale Upper Surface Blown-Flap Model Having Four Engines," NASA TM X-62,419, July 1975.

28. Aiken, T. N., Aoyagi, K., and Falarski, M. D., "Aerodynamic Characteristics of a Large-Scale Model with a Swept Wing and Jet Flap Having an Expandable Duct," NASA TM X-62,281, Sept. 1973.

29. Butler, S. F. J., Guyett, M. B., and Moy, B. A., "Six-Component Low-Speed Tunnel Tests of Jet-Flap Complete Models with Variation of Aspect Ratio, Dihedral, and Sweepback, Including the Influence of Ground Proximity," RAE Report No. Aero. 2652, June 1961.

30. Aiken, T. N. and Cook, A. N., "Results of Full-Scale Wind Tunnel Tests on the H.126 Jet Flap Aircraft," NASA TN D-7252, April, 1973.

31. Unpublished Lateral Directional Data Courtesy of David Taylor Naval Ship R&D Center from the Program Reported in: Englar, R. J., "Development of the A-6/Circulation Control Wing Flight Demonstration Configuration," DTNSRDC/ASED-79/01, January 1979.

D I S T R I B U T I O N L I S T

REPORT NO. NADC-81275-60

AIRTASK NO. A03V-320D/001B/7F41-400-000

	No. of Copies
NAVAIR (AIR-950D)	4
(2 for retention)	
(1 for AIR-320D)	
(1 for AIR-5301)	
NAVWPNCEN, China Lake, CA	1
NAVAIRPROPCEN, Trenton, NJ	1
DTNSRDC, Bethesda, MD (Attn: Dr. H. Chaplin & R. S. Englar)	2
ONR, Arlington, VA (Attn: R. Whitehead)	1
NAVPGSCOL, Monterey, Ca (Attn: M. Platzer)	1
NASA, Ames Research Center, Moffett Field, CA	2
(1 for D. Koenig)	
(1 for W. Decket)	
NASA, Langley Research Center, Hampton, VA	2
(1 for J. Chambers)	
(1 for R. Margason)	
NASA, Lewis Research Center, Cleveland, OH	1
Wright-Patterson AFB, Dayton, OH	2
(1 for Flight Dynamics Lab)	
(1 for Aeronautical Systems Division)	
The Pentagon, Washington, DC (Attn: R. Siewert)	1
U.S. Army Aviation Systems Command, St. Louis, MO	1
U.S. Army Research Office, Durham, NC	1
DTIC, Alexandria, VA	12
Boeing Company, Seattle, WS (Attn: D. E. West)	1
LTV Aerospace Corporation, Dallas, TX	2
(1 for T. Beatty)	
(1 for W. Simpkin)	
Rockwell International, Columbus, OH (Attn: W. Palmer)	1
General Dynamics Corporation, Ft. Worth, TX (Attn: W. Folley)	1
Nielson Engineering, Mountain View, CA (Attn: S. Spangler)	1
Univ. of Tennessee, Space Inst., Tullahoma, TN (Attn: W. Jacobs)	1
Lockheed-California Co., Burank, CA (Attn: Y. Chin)	1
Northrup Corporation, Hawthorne, CA (Attn: P. Wooler)	1
Grumman Aerospace Corp., Bethpage, LI, NY (Attn: S. Kalamaria)	1
Royal Aeronautical Establishment, Bedford, England (Attn: A. Woodfield)	1
Fairchild-Republic Corporation, Farmingdale, LI, NY	1
Calspan, Buffalo, NY	1
McDonnell Douglas Corp., St. Louis, MO (Attn: Dr. D. Kotansky)	1
R. Kuhn, Newport News, Va	1
Georgia Inst. of Technology, Atlanta, GA (Attn: Dr. H. McMahon)	1
Penn State Univ., Univ. Park, PA (Attn: Prof. B. W. McCormick)	1
Douglas Aircraft Co., Long Beach, CA (Attn: E. R. Heald)	1
General Dynamics, Convair Div., San Diego, CA (Attn: M. B. Eilert, Jr.)	1
Lockheed Georgia Co., Marietta, GA (Attn: L. R. Woodward)	1
NASA Headquarters, Washington, DC (Attn: W. Aiken)	1
NASA, Dryden Research Center, Edwards AFB, CA (Attn: T. Ayers)	1

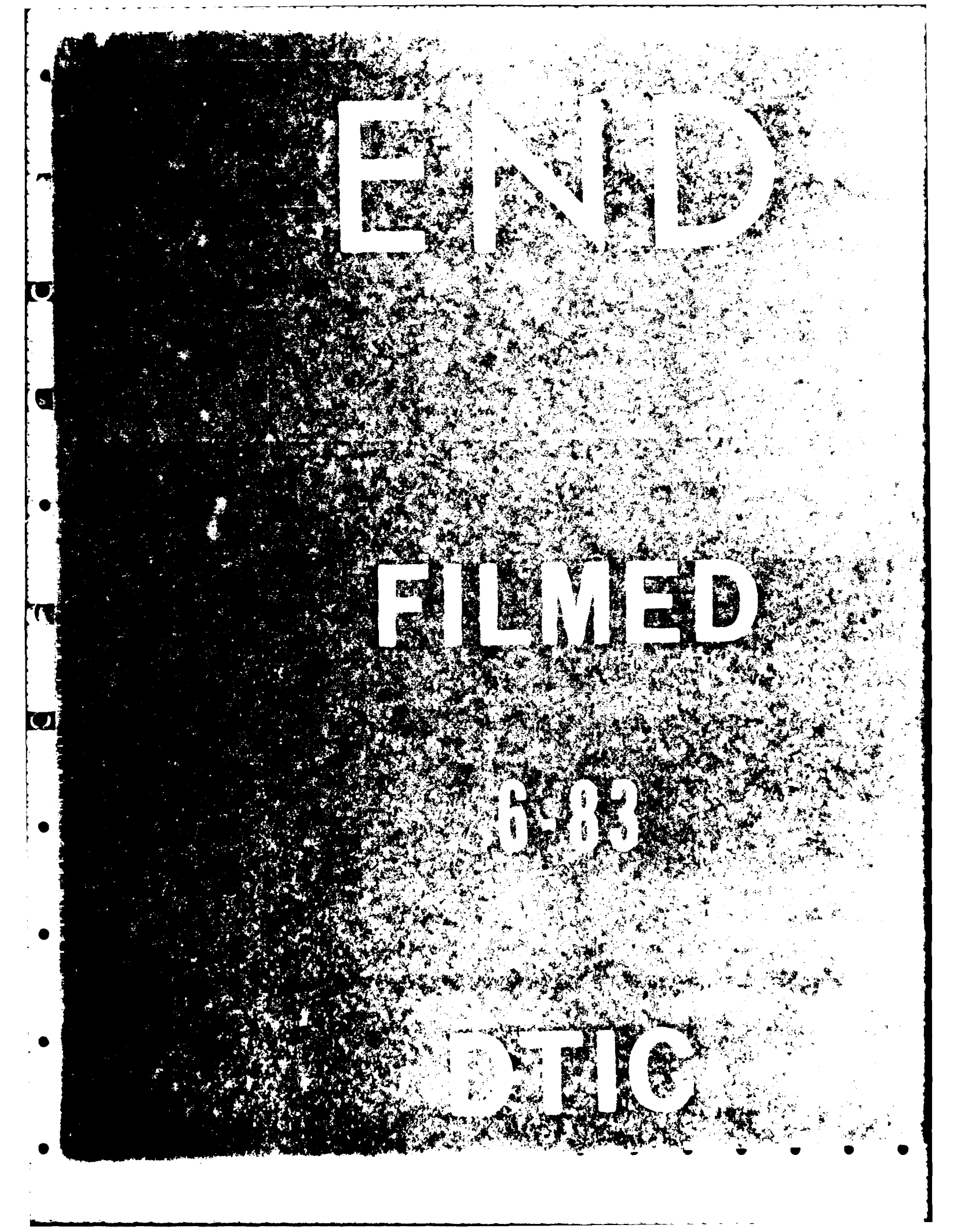
END
FILMED
6-83
DTIC